MECHANICAL PROPERTIES OF SUPERPLASTIC Al-Zn ALLOYS

NEAR THE TRANSITION REGION

A THESIS

Presented to

The Faculty of the Division of Graduate

Studies and Research

By

S. A. Hamid Ghazanfar

In Partial Fulfillment

of the Requirements for the Degree

Master of Science in Mechanical Engineering

Georgia Institute of Technology

December, 1973

MECHANICAL PROPERTIES OF SUPERPLASTIC Al-Zn ALLOYS

NEAR THE TRANSITION REGION

Approved:

E. E. Underwood, Chairman

David Kalish

E. A. Starke

Date approved by Chairman: 28 Nov 73

I dedicate this thesis to my loving father, who has always encouraged me in my efforts to obtain a fine education and bravely endured my absence from his side.

ACKNOWLEDGMENTS

TABLE OF CONTENTS

LIST OF TABLES

LIST OF ILLUSTRATIONS

Figure   Page

LIST OF SYMBOLS

Symbol

ℓ_o	Original gage length
ℓ	Instantaneous length
ℓ_u	Length at the point of maximum load
A	Instantaneous cross sectional area
A_u	Cross sectional area at the point of maximum load
F	Force
P	Load
$\bar{\sigma}$	True stress
$\bar{\sigma}_u$	Ultimate stress
$\bar{\varepsilon}$	True strain
$\dot{\bar{\varepsilon}}$	True strain rate
t	Time
m	Strain rate sensitivity index
K	Strain rate hardening constant
k	Boltzmann's constant
Ω	Atomic volume
d	Grain size
Γ	Grain boundary free energy
D_v	Bulk diffusion coefficient
D_B	Boundary diffusion coefficient
δ	Thickness of the boundary

Symbol

T	Temperature °C, unless specified otherwise
T_c	Invariant temperature
μ	Shear modulus
μm	Micron
b	Burgers vector
Q_c	Activation energy
D_i	Inside diameter
$\bar{L}$	Mean intercept length
R	Gas constant
V_v	Volume fraction
V	Velocity
P_L	Number of grain boundary intersections per unit length of test line
α	Aluminum-rich phase
β	Zinc-rich phase
$\P$	Combined parameter of T and $\dot{\varepsilon}$

SUMMARY

The question addressed by this investigation is whether the superplastic state is uniquely characterized by its own mechanism of deformation, or whether it results merely from a gradual transition between high-temperature creep and slip mechanisms. In order to determine the nature of the transition, the mechanical properties of Al-78 wt % Zn alloys were studied by tensile tests over a range of temperatures and strain-rates that included the maximum superplastic effects. Microstructural changes were also followed in deformed alloys by scanning electron microscopy and quantitative microscopy.

The trend of the basic log stress-log strain rate curves indicated gradual changes in slope from the maximum superplastic region to the low and high stress regimes. Other parameters such as the strain rate sensitivity index m, and the total elongation showed that transition from the superplastic to the non-superplastic state is a gradual process. The dependence of stress upon a combined parameter of temperature and strain rate, $\sigma = f[T(C-\log\dot{\varepsilon})]$, also showed a gradual transition from the superplastic state, as did the microstructural changes in the deformed alloys.

These results lead us to the conclusion that superplasticity in Al-78 wt % Zn alloys is not identifiable as a

sharp transition region. Rather there is a gradual change in
relative contribution of slip and diffusion-controlled
processes, resulting in a region of optimum interaction with
the grain boundary sliding mechanism of deformation. In
this region the maximum superplasticity is observed.

CHAPTER I

INTRODUCTION

Superplasticity is a metallurgical phenomenon which has been a major subject of research over the past ten years. It is identified as the state in which metals exhibit remarkably large deformation under extremely small forces with an unusual capacity to resist necking. A growing number of metal systems are being found that exhibit this type of behavior.

It is now established that superplasticity in metal alloys requires a very fine grain size, moderate strain rates, and working temperatures of more than about half the absolute melting point.

Numerous studies of high temperature tensile behavior have shown that distinct mechanisms of deformation are dominant at high or low strain rates. It is also generally agreed that the mechanism dominating superplastic deformation is grain boundary sliding (GBS). Experimental evidence has shown that at high strain rates (low temperatures), the primary mechanism controlling the deformation is slip, while at low strain rates (high temperature), the dominant mechanism is diffusion creep. In between there is a transition region in which GBS becomes evident.

In this investigation the objective is to define the properties and characteristics of this transition region. The Al-78 wt. % Zn eutectoid alloy has been selected for this study. Tensile tests are conducted at various strain rates and temperatures close to the superplastic region. Along with the transition region study, metallographic studies are made to determine the microstructural conditions that produce the superplastic state.

Before further discussion of the results of these tests, a historical review on the subject of superplasticity is presented as well as the results of the latest investigations in the field.

CHAPTER II

BACKGROUND

The deformation of high strength, high temperature
materials under low loads has been a long sought goal, and
research pursuing this objective has been underway on a
broad front.

A notable case is the early work of Sauveur [1] who
demonstrated unusual softening and plasticity in torsion
tests of iron bars in a longitudinal temperature gradient.
The regions of easy twisting were found to be at the trans-
formation temperatures. In 1934, Pearson [2] reported
elongation of 1950% in eutectic bismuth-tin, tested at room
temperature. Both these observations are believed to be
manifestations of the superplasticity phenomenon.

Along this line of research, Bochvar [3], in hot
hardness studies of aluminum-zinc alloys, aroused interest
in the phenomenon for which he coined the term "super-
plasticity." The subject was further investigated by
Presnyakov and other Russian metallurgists [4,5,6] who
studied many alloys, especially the binary alloys of aluminum.
The Soviet investigators postulated that superplasticity was
associated with a phase change process called the solution-
precipitation theory. Presnyakov [4] showed that the

eutectoid Al-Zn alloy, when solution treated and quenched, had a finely dispersed microstructure. He postulated that the metastable phase formed upon quenching would transform to the equilibrium structure with increasing temperature and an externally applied stress. This would give rise to the phenomenon of superplasticity. In another study Presnyakov and his associates [5] attempted to correlate superplasticity in eutectic alloys with the extent of metastability of the quenched structures. No systematic correlation was found. Their proposed mechanisms, however, have been shown to be inadequate [7].

During the early 1960's the phenomenological studies of superplasticity aroused American interest, which began with the paper of Underwood [8], who published a review primarily of the Soviet investigations. Other reviews of superplasticity have appeared as the number of research investigations have increased. Johnson [9], in 1970, reviewed the experimental and practical results, as did Davies, et al. [10] the same year. In 1972, Nicholson [11] summarized the literature, and emphasized the metallographic contributions to the understanding of superplasticity.

Some of the more recent works that summarize the phenomenological and experimental background status of superplastic research are discussed next. We then proceed to a discussion of mechanisms currently under consideration, as well as the unresolved problem of the accommodation

process(es) that control the rate of grain boundary sliding.

Backofen, et al. [12], working with Al-80% Zn alloy, proposed that the stretching behavior of superplastic alloys is a consequence of Newtonian viscosity, in which there is a direct proportionality between flow stress and strain rate, independent of the strain. The necking resistance of super-plastic alloys was thus correlated with strain rate hardening. For the correlation, the strain rate sensitivity index m was evaluated according to the equation:

$$\bar{\sigma} = K\dot{\bar{\varepsilon}}^m \qquad (1)$$

where $\bar{\sigma}$ is the true stress, $\dot{\bar{\varepsilon}}$ the true strain rate, and K is a constant. On a logarithmic plot m becomes the slope of the curve log $\bar{\sigma}$ vs. log $\dot{\bar{\varepsilon}}$, or m = d log $\bar{\sigma}$/d log $\dot{\bar{\varepsilon}}$. For Newtonian viscous flow, m is unity; in Backofen's experiment m was found to be maximum (about 0.6) for test temperatures between 220 to 260°C, and strain rates of about 1 min.$^{-1}$ (Figure 1). Their results are supported by the following mathematical argument:

$$\bar{\sigma} = K\dot{\bar{\varepsilon}}^m = \frac{F}{A} \qquad (2)$$

where F is the applied tensile load transmitted through the cross-sectional area A. The strain rate at any point along the gage length is:
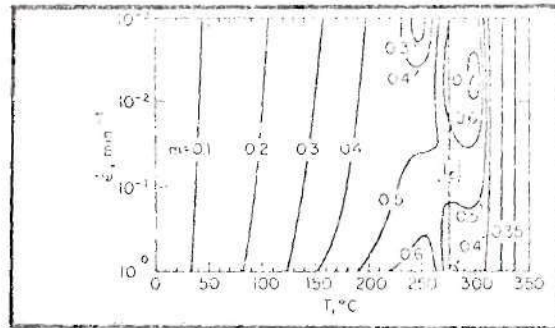
Figure 1. Topographic Map of the m-ė-T Surface
(Contour lines are drawn for constant
m. T_c = critical temperature. The
data was taken from Al-80% Zn alloy.)
After Backofen [12]

$$\dot{\varepsilon} = \frac{1}{\ell} \frac{d\ell}{dt} = -\frac{1}{A} \frac{dA}{dt} \qquad (3)$$

By combining Equations (2) and (3) and rearranging, the following is obtained:

$$\frac{dA}{dt} = -\left[\frac{F}{K}\right]^{\frac{1}{m}} [A]^{\frac{m-1}{m}} \qquad (4)$$

From Equation (4) it can be seen that for m = 1, dA/dt is independent of A and neck growth is minimized, i.e., the rate of reduction of all cross sections along the gage length is a constant value. However, for m values much smaller than unity, the cross section of a small area decreases more rapidly than a large area, which leads to local necking. Values of o<m<l determine the rate at which necking occurs and accounts for the possibility that superplasticity is primarily a slow necking process.

Holt [13], in compression tests on Al-Zn eutectoid alloys, attempted to show that m values arise from grain boundary shear. His prepolished specimens were inscribed with fine longitudinal scratches. Compression at 250°C caused the scratches to be offset at grain boundaries. The offsets were measured, and the relative grain boundary shear was calculated. The latter is plotted in Figure 2 versus strain rate, showing a maximum contribution of about 60% to the total strain. This maximum coincides with the maximum
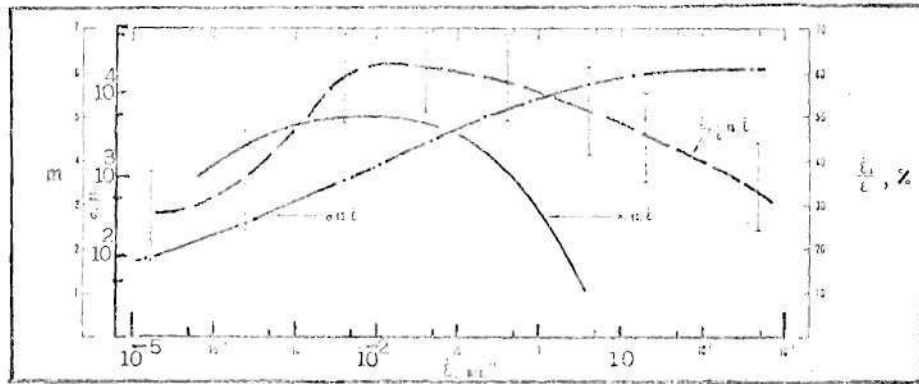
Figure 2.   Dependence of the Contribution of Grain Boundary
           Shear to Total Strain $\varepsilon_s/\varepsilon$, on Strain Rate, $\dot{\varepsilon}$,
           for Al-78 wt % Zn Alloy. (Temperature is 250°C,
           Stress, σ, and strain rate sensitivity index, m,
           are also plotted against strain rate.)
           After Holt [13]

in m. Further microstructural study showed that grain boundary migration smoothed the boundaries and relieved stress concentrations at triple lines, and was accounted as an accommodation process for GBS.

Alden [14] also inscribed a set of straight grid lines on a polished surface of his Sn-Bi specimens before deformation. The sharp offsets at grain boundaries and lack of curvature of the scribed lines after deformation was good evidence for grain boundary sliding.

The determination of the mechanisms involved in superplastic deformation has been studied widely on a variety of metals. In an early study of Pb-Sn alloys, Backofen and Avery [15] propose that the mechanisms controlling the deformation consist of two competing processes: Nabarro-Herring (N-H) creep and climb of dislocations. Later, however, their proposal was refuted by Backofen and Holt [16], as well as by Alden [14] et al., because the N-H creep mechanism changes the grain shape, while in superplastic deformation the grain size and shape remain unchanged. In their reconsideration [16], a viscous boundary shear was preferred as the principal mechanism with grain boundary migration as the accommodation process to reduce mechanical obstructions, i.e., unfavorably oriented grains, ledges and sharp grain corners.

Alden [14] found in his study of Sn-Bi alloys that distinct mechanisms of deformation are dominant at low and high strain rates. At low strain rates grain boundary sliding

is dominant, while the dominant high strain rate mechanism is slip. The region of transition in which GBS becomes an important deformation mode is associated with the maximum rate sensitivity m. He concluded that grain boundary migration was the accommodation mechanism for GBS.

Hayden [17], agrees that the predominant process of deformation in superplasticity is GBS, but that the overall deformation is governed by transgranular dislocation climb. His results show that at any temperature and low stress levels, diffusion creep is the predominant and rate controlling mechanism. At higher stresses in fine grain materials, GBS would be rate controlling. This would be the superplastic state. At still higher stress, dislocation creep would dominate the process.

Obstructions to GBS have been analyzed in detail by Ashby and Raj [18]. They proposed that the rate of sliding on a stressed grain boundary is determined by boundary shape. Their model assumes wavy and stepped grain boundaries, in two and three dimensions, and nonplanar grain boundaries that lock the two adjacent grains together against the applied shearing stress.

At low temperatures, elastic deformation occurs, which would ultimately be stopped when the internal stress balances the applied stress. With the removal of the applied stress the displacement would be recovered. At higher temperatures diffusional flux of atoms and vacancies accommodates a

permanent boundary sliding, by means of mass transfer from the compressed points to those in tension.

In a later paper, Ashby and Verrall [19] explain the details of a grain-sliding mechanism, based on a two-dimensional model. With the aid of "an oil emulsion analog," they visualized a group movement of grains in which the neighbor-switching event is the main feature. In their model, the unit step of deformation involves the sliding of four grains from a position as shown in the left of Figure 3, to the final position as shown in the right of Figure 3. This has been called a pinch-pull boundary migration mechanism [21]. Idealization of the process is described by the sequence from initial state to the final in Figure 3. The initial state shows that grains 2 and 4 are adjacent grains. A constant tensile stress applied in an isothermal process, causes all four grains to come in a common neighborhood, i.e. intermediate state. Further stretching from this temporary state leads to the final state. In this state grains 1 and 3 are adjacent. The net effect is that this movement of grains has resulted in a 55% permanent elongation in the direction of the tensile load, without changing grain shape.

They propose [19] that the strains required when the grains switch from the initial to the intermediate positions are accommodated by bulk diffusion or boundary diffusion. Changes in shape are obtained predominantly through grain
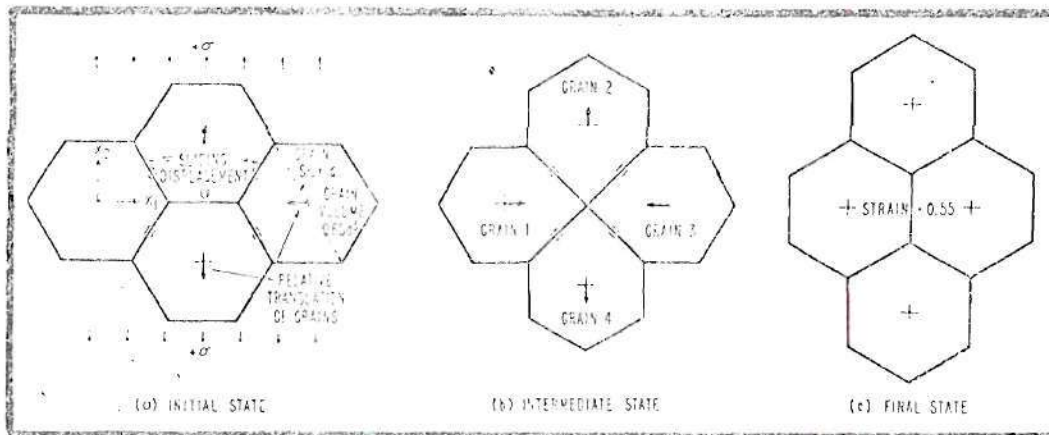
Figure 3. Unit Step of the Deformation Process. (A group
of four grains move from the initial through
the intermediate state to the final state. The
initial and final states of the polycrystal are
thermodynamically identical, although it has
suffered a true strain $\varepsilon = 0.55$. In so doing,
the grains suffer accommodation strains and
translate past each other by sliding at their
boundaries.) After Ashby [19]

boundary diffusion, as shown in Figure 4.

The review up to this point reveals that GBS is the basic and principle mechanism in superplasticity. Each investigator also concludes that GBS is insufficient for superplastic deformation without accommodation processes. Backofen [16], Alden [14] and Holt [13] consider boundary migration to be the accommodation process that permits boundary sliding. Ashby and Raj [18] propose that grain boundary diffusion is rate controlling in the accommodation process. Hayden [17] proposes that dislocation creep is the rate controlling mechanism for GBS.

Ashby and Verrall [19] have brought together the divergent views on an accommodation process, and presented a rationale of a general nature. They theorized that superplastic deformation is the result of nonuniform flow and that GBS is the principle flow mechanism with diffusional or interface reactions acting as the accommodation process.

Their proposal recognizes that grain boundary sliding could produce only very small strains without the accommodation process. Thus for the elongation obtained by the neighbor-switching sequence, four irreversible processes would contribute. Figure 4 shows the description of the processes taking place on one face of two grains, as follows:

1. Diffusive process on the boundary as a high conductive path.

2. The interface reaction for vacancy removed or added to the boundary.
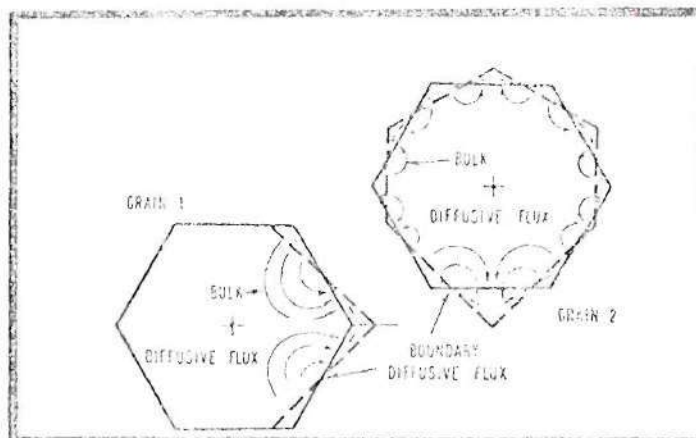
Figure 4. Proposed Diffusion Accommodation of Strains in Grain Boundary Sliding. After Ashby [19]

3. Grain boundary sliding or translation of grains passing each other.

4. Grain boundary migration or fluctuation of boundary area.

Each of the processes dissipate power internally, which predict the amount of energy required for superplastic deformation. The energy rate consumption of all four processes are formulated, combined and correlated with applied stress, strain rate and temperature [20]. The result is:

$$\dot{\varepsilon}_{\text{D-A flow}} = 100 \, \frac{\Omega}{kTd^2} \{\sigma - \frac{0.72\Gamma}{d}\} D_V (1 + \frac{3.3\delta}{d} \frac{D_B}{D_V}) \quad (5)$$

where $\dot{\varepsilon}$ = tensile strain rate, σ = tensile stress, Ω = atomic volume, d = grain size, Γ = grain boundary free energy, D_V = bulk diffusion coefficient, δ = thickness of the boundary, T = absolute temperature, k = Boltzmann's constant, and D_B = boundary diffusion coefficient. Equation 5 is similar to the N-H and Coble creep equations, but the calculated rate from Equation 5 compares well with experiments, while the other two theories predict a creep rate an order of magnitude too low. In superplastic deformation, or when GBS is the dominant mode, Equation 5 describes the mechanical behavior of the flow. But in an overall flow process, alternative mechanisms come into play. The most common and independent competing mechanism is dislocation creep. The equation describing flow by dislocation creep is given as

$$\dot{\varepsilon}_{\text{dislocation creep}} = A_1 \frac{\mu b}{kT} \left(\frac{\sigma}{\mu}\right)^n \exp - \frac{Q_c}{kT} \qquad (6)$$

where k and T are the same as in Equation 5, μ = shear
modulus, b = Burgers vector, Q_c = activation energy. A_1
and n are empirical constants.

Since the two competitive processes of diffusion-
accommodated flow and dislocation creep can occur to some
extent simultaneously, the overall creep rate $\dot{\varepsilon}_{\text{total}}$ can
represent the superposition of both; that is

$$\dot{\varepsilon}_{\text{total}} = \dot{\varepsilon}_{\text{D-A flow}} + \dot{\varepsilon}_{\text{dislocation creep}},$$

or

$$\dot{\varepsilon}_{\text{total}} = 100 \frac{\Omega}{kTd^2} \{\sigma - \frac{0.72\Gamma}{d}\} D_v (1 + \frac{3.3\delta}{d} \frac{D_B}{D_v}) + A_1 \frac{\mu b}{kT} \left(\frac{\sigma}{\mu}\right)^n \exp - \frac{Q_c}{kT} \quad (7)$$

where the terms are defined above.

Ashby summarizes his argument by means of a calculation
which is based on data for lead. The curve in Figure 5 is
divided into three regimes, according to the relative
contributions made by each mechanism to the flow stress. In
the low stress regime diffusion accommodated flow is dominant.
Deformation occurs without large elongations of the grains.
Due to translation and rotation of the grains, any textures
or obstructions on the boundary are destroyed. m rises from
a low level and reaches a maximum value which occurs at a

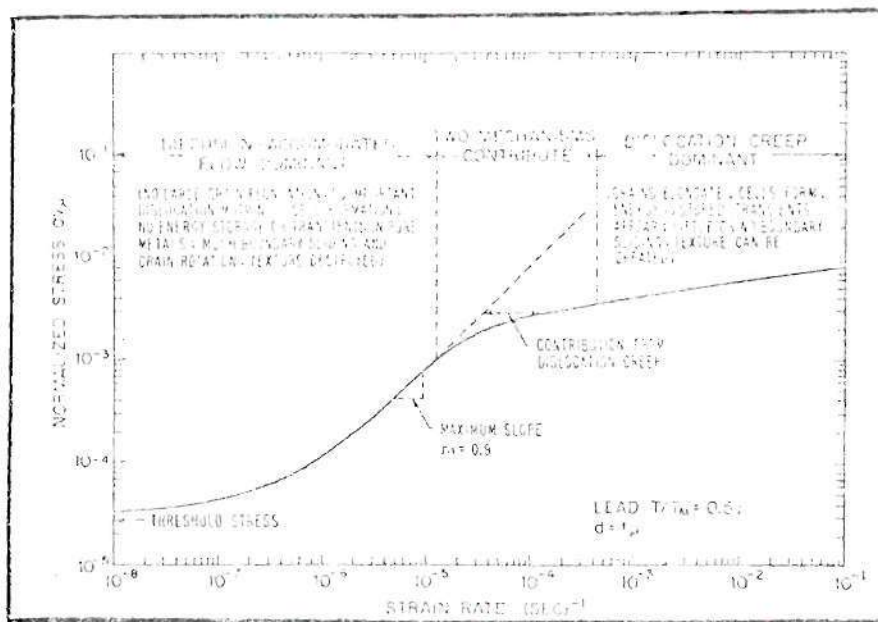Figure 5.   Plot of the Equation for Plastic Flow of
            Polycrystaline Lead (Equation 7). (The
            plot shows the super-position of two
            mechanisms: diffusion accommodated flow
            (Equation 5) and dislocation creep
            (Equation 6). The microstructural and
            other characteristics of each mechanism
            are listed.) After Ashby [19]

strain rate that depends heavily on microstructure and test temperature. The maximum m is due to a sudden rise from the low stress regime, or a sudden drop from the high stress regime. This is thought to be when the highest percentage of strain is accomplished by grain boundary sliding [12,14, 21]. In the high stress regime dislocation creep dominates the flow. Dislocations move through the grains and accumulate as cells or tangles, storing energy. Due to slip, grains elongate and change shape considerably. In the intermediate stress regime the two mechanisms contribute and control the flow rate. Grains elongate but not as much as the specimen itself. Ashby believes that for large strains in this regime the two mechanisms will not be linearly additive. "This is because the dislocation-creep component will interfere with the grain switching mechanism. The net result is simply to narrow this intermediate-stress regime" [19] (with regard to strain rate).

The latter statement bears heavily on the central issue of this thesis. That is, whether the transition from GBS to the high stress regime takes place abruptly or gradually, in other words, we wish to determine whether the curve of log σ versus log $\dot{\varepsilon}$ gives a sharp transition or a smooth one. This question is also of concern to Nicholson [11], who concludes that there is a definite range of testing conditions under which superplasticity is found. In his opinion, it is not a transition phenomenon between two

separate deformation mechanisms. Alden [14], on the other hand, describes superplasticity to a transition region between GBS and slip. Other authors [22] also show that the transition from GBS to slip as the dominant deformation mode occurs in a relatively narrow range of strain rates.

Experimental evidence by Hayden, et al. [23] gives **striking** support to the sharp transition theory. Their curve is reproduced in Figure 6, showing only two linear portions of the curve of log stress versus log strain rate, over about five orders of magnitude. The experimental observations are summarized by Hayden and Brophy [24], and shown here in Figure 7.

Thus, it can be seen, there is a wide body of disagreement as to the exact nature of the transition into the superplastic state. It is the purpose of this thesis to examine the region of maximum superplasticity in order to shed some light on the nature of the transition region. This can be determined by tensile tests at various strain rates and temperatures close to the transition region, as well as a study of the corresponding microstructural conditions before and after the transition. These two parallel studies are to be the basis of the following experimental research.
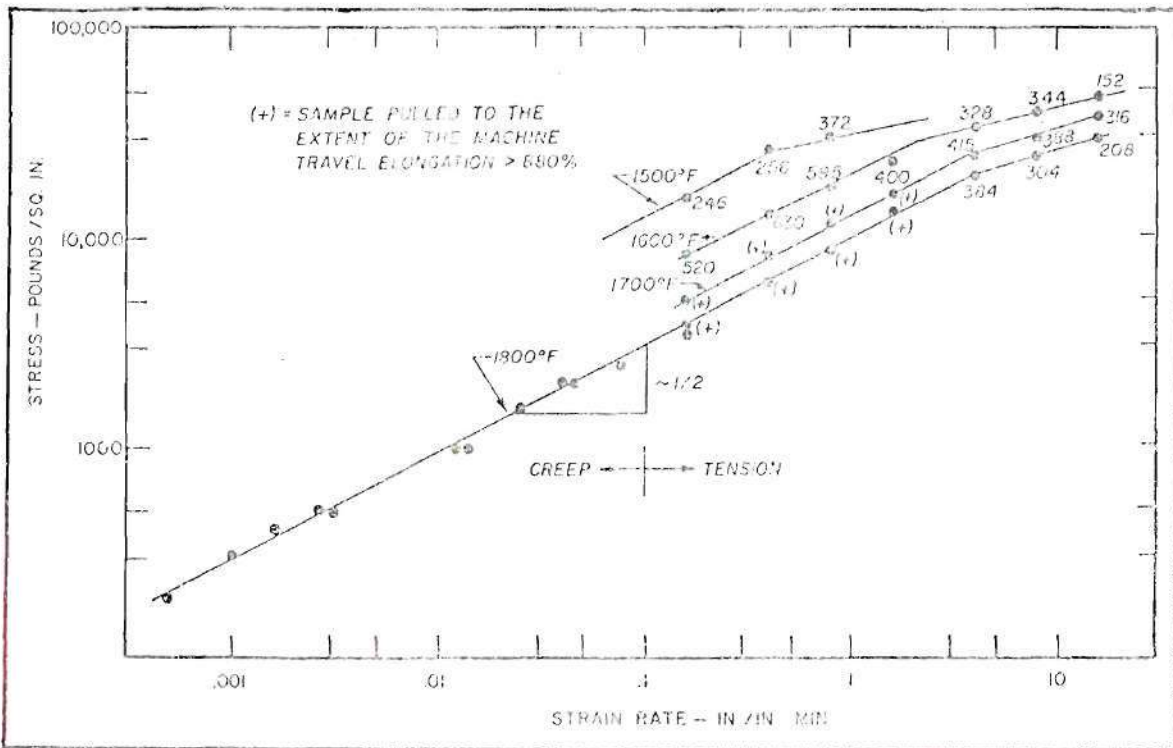
Figure 6. Stress Versus Strain Rate for a 39% Cr-10% Fe-
1.75% Ti-1% Al-bal Ni Alloy. (Numbers beside
each point represent elongation at rupture.)
After Hayden [23]
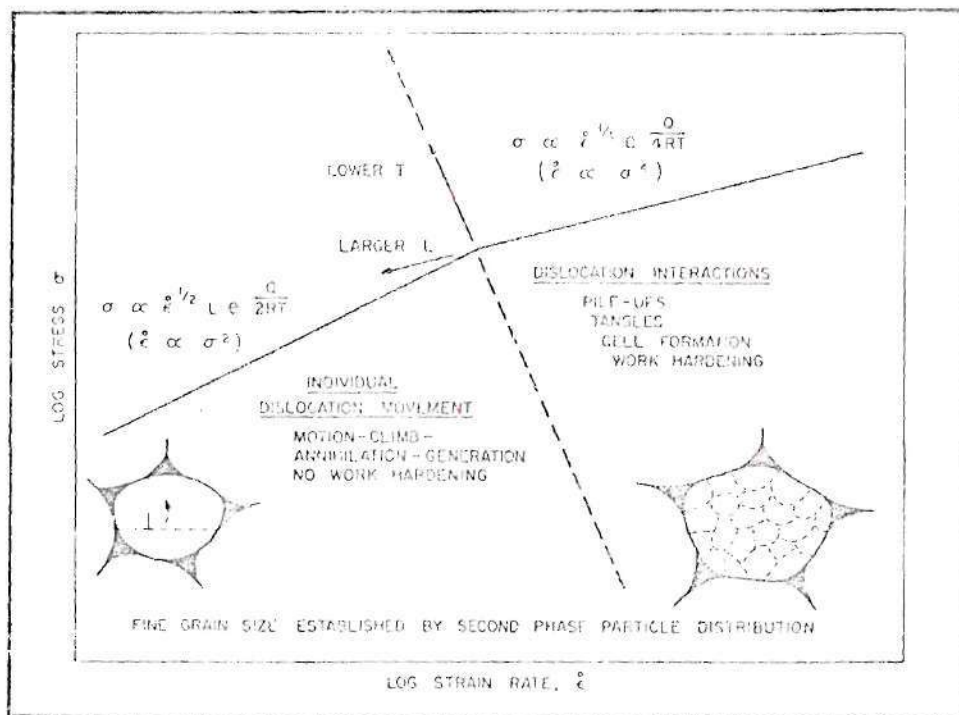
Figure 7. Schematic Stress Versus Strain Rate Relation Summarizing Experimental Observations and the Mechanism of Deformation. After Hayden [24]

CHAPTER III

EXPERIMENTAL PROCEDURES

A. Material

The Al-Zn eutectoid alloy used in this research program was prepared through the courtesy of the Ball Corporation of Muncie, Indiana, from high-purity Al and Zn. The material was received in the form of 1/4-inch thick hot rolled plates. Square rods of 1/4" x 1/4" were cut from the plate and homogenized at 375°C for 50 hours. The sharp edges of the rods were rounded off before swaging them to 0.147-inch diameter rounds to eliminate any possible porosity or flaws.

The specimens made from the swaged wires had a composition of 78.1 $\pm$ 0.2% Zn and 21.5 $\pm$ 0.3% Al by weight as determined by wet chemical analysis. The dimensions of the specimen are shown in Figure 8. The initial gage length was taken to be 1 inch, the full distance between the specimen shoulders.

Specimens were prepared in two batches for comparison of grain size effects.

Batch A. Solution treated at 375°C then quenched to room temperature in brine bath.

Batch B. Solution treated at 375°C, brine quenched to room temperature, then aged at 250°C for 6 days, followed by another brine quench.
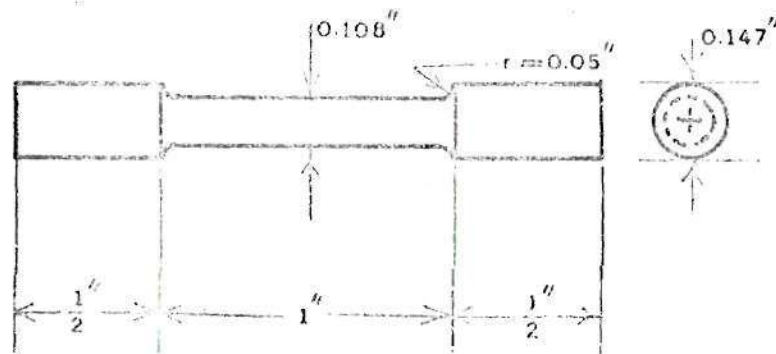
Specimen Dimensions
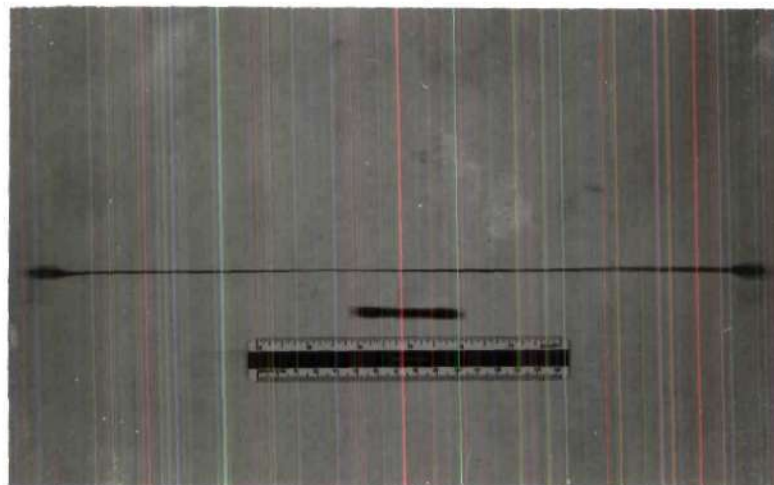
Figure 8. Illustration of Stretching in Specimen No. 36.
(The specimen was annealed at 375°C for 50 hr.,
quenched to room temperature, and then pulled
at 250°C at a strain rate of 1 min⁻¹. The
total elongation was 1238%. A 6 in. scale
with an undeformed specimen is shown for
comparison.)

B. Mechanical Testing

Tensile tests were performed on an Instron machine equipped with an Instron furnace (environmental chamber) 18 inches long. Crosshead velocities of only 0.02 to 20 in/min. were available, which restricted the choice of grain sizes that could be used, since it was desired that the transition region should fall within the available range of crosshead velocities.

A total of 60 specimens from batch A were tested at six temperature levels ranging from 178 to 272°C, the latter just below the invariant temperature of 275°C. Ten specimens of batch B were tested at 250°C for comparison with batch A at that temperature. Tests were made at ten crosshead speeds between 0.02 to 20 in/min. The ratio of any two successive levels was either 2 or 2-1/2. Some specimens of batch A were tested using a procedure that involved sudden changes in rate, including three specimens that were pulled in the single phase region at 285°C. The selected test temperatures near the transition region were closer than those elsewhere. For every specimen the load P was measured for its maximum value. The time required for each specimen to reach a constant test temperature in the furnace was 35 minutes.

A special gripping system was designed and fabricated from stainless steel. Figure 10 shows essential elements of the system. Prior consideration in the design were the
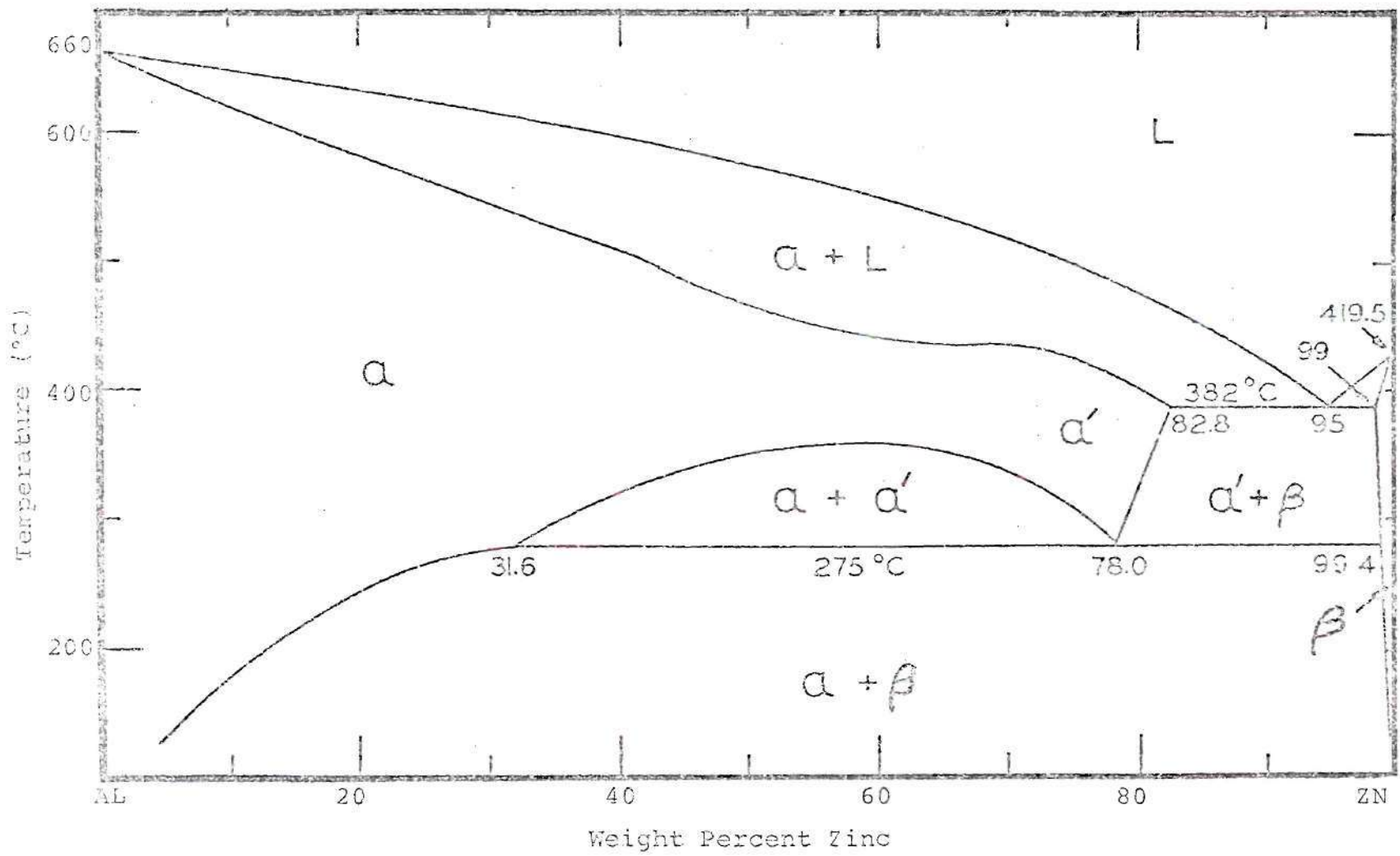
Figure 9. Aluminum-Zinc Phase Diagram, from the New Jersey
Zinc Company Publications, 1972.

To the
Load cell

To the Crosshead

S. Specimen
A. Thermocouple Upper Shoulder
B.   "   Lower   "
C.   "   Mid Point
G. Grip and Grip Jaws
N. Lock Nut
R. Ring Closing the Jaws
P. Protection Collar
W. Thermocouple Wiring
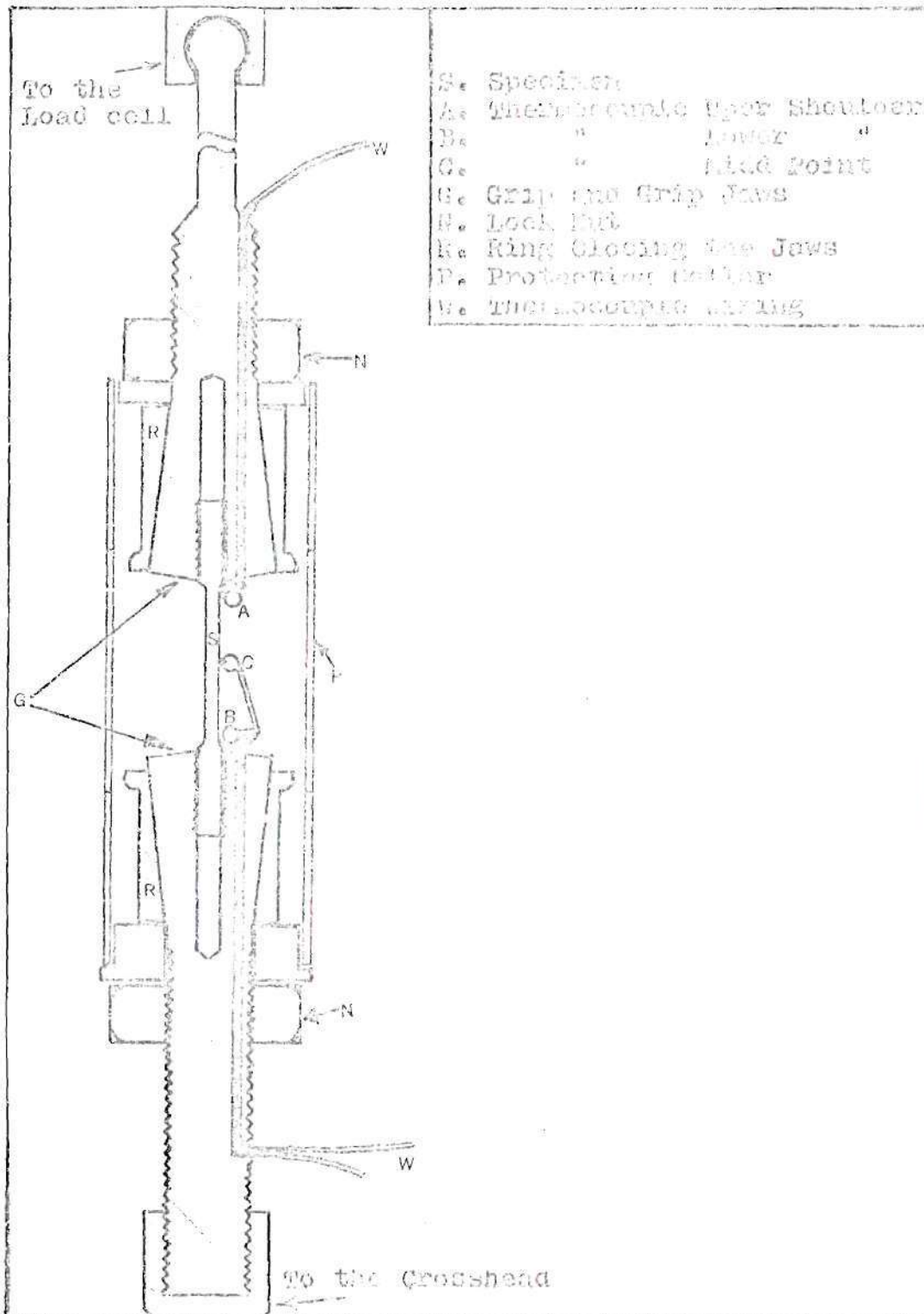
Figure 10.   Longitudinal Cross Section of Gripping Assembly

prevention of slippage of the specimen from the grips, stress concentrations on the specimen and oxidation of the specimen surface between the grip and the specimen, as well as an easy way to insert and remove the specimen from the grips.

Specimens could be placed between the grip jaws easily and smoothly without any bending or twisting force being exerted on the specimen, which might cause critical damage to the small size specimen. In order to roughen the inside wall, a tap was turned inside the grip hole to make a shallow thread, then the jaws could be locked firmly by means of a lock nut that tightened a ring around the jaws.

In order to hold the specimen straight and aligned between the grips, a steel collar was fitted around the two grips. This was an effective way to protect the specimen from damage during placement inside the hot furnace. The linkages to connect the gripped specimen to the load cell and crosshead of the Instron were made from 1/4" diameter stainless steel rods. They were turned to optimum diameters for the best heat conduction control.

Some modification was done on the furnace and tube to provide for establishment of a uniform temperature gradient along the length of the tube. Figure 11-a shows the arrangement schematically. A 1.5" (D_i) steel pipe was machined and fitted into the center of the furnace with ten thermocouple beads mounted about 1.5" apart along the pipe and suspended inward from small windows premachined along the pipe.
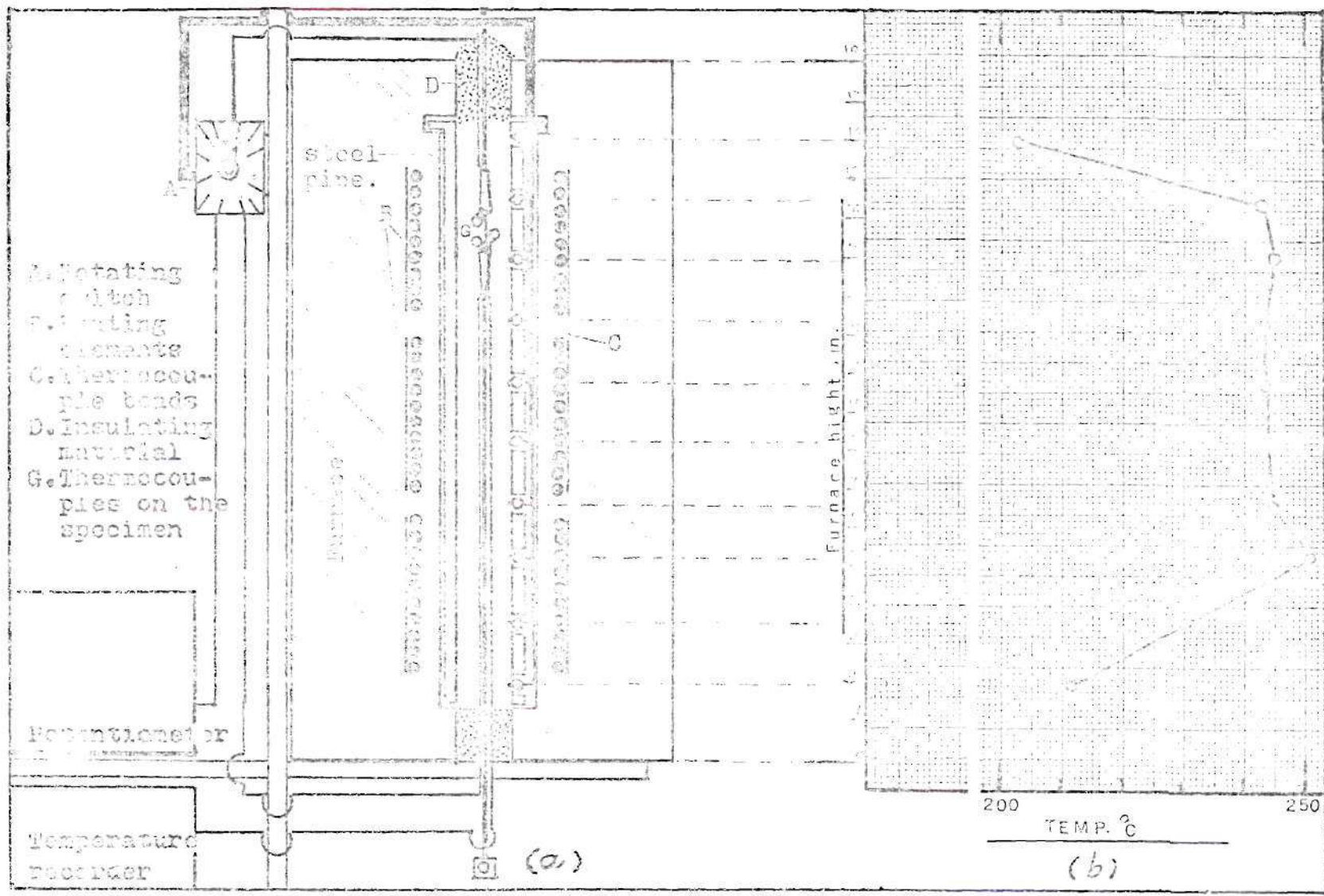
Figure 11. (a) Cross Section of the Modified Furnace. (b) Temperature Gradient Versus Length Along the Furnace.

Three additional thermocouples were attached closely at the top shoulder, bottom shoulder and middle of the gage length of the specimen. All thermocouples were wired to a potentiometer across a rotating switch, except the one at the middle of the gage length, which was connected to a temperature recorder.

Three independent heating elements, controlled through separate circuits and variacs, were coiled around the pipe at the top, middle, and bottom of the furnace. All these arrangements made it possible to establish a uniform temperature for at least eight inches at the middle along the center of the furnace. Figure 11-b shows a plot of the temperature variation inside the heated pipe before each test was begun. The temperature was controlled at the shoulders of the specimen within $\pm 2°C$, while the longitudinal temperature variation was 4-5°C along the fully stretched specimen.

C. Metallography

Photomicrographs of the tensile specimen microstructures were taken both by light and electron microscopy. Metallographic examination was done on selected portions of the gage length on longitudinal sections. Standard polishing techniques [26,27] were used, with samples being mounted on cold mounts for its low curing temperature. Etching was accomplished either by a 3-second immersion in a solution of $0.15\%HF+0.35\%HNO_3+99.5\%H_2O$ [25] or a 20-second immersion in

0.3%HF+99.7%H$_2$0 (all in volume percent). Electron micrographs were taken by scanning electron microscopy of selected fields of view after microscopical examination.

CHAPTER IV

EXPERIMENTAL RESULTS

Tensile Testing

A. Load-Elongation Curves

Some typical curves of tests conducted under constant crosshead velocities or under sudden changes in velocity are shown in Figure 12. Generally for all tests, the load reached its peak value as soon as pulling was started. No well defined elastic strain was measurable, so purely plastic flow was assumed. Keeping the test temperature constant, for velocities V > 1 in/min the load would reach a sharp maximum point, then decay with a concave upward slope, (Figure 12-a). For velocities V < 1 in/min the load would rise to a broad rather than sharp maximum and then decay with a slower rate, (Figure 12-b). For fixed velocities, the curves obtained at higher temperatures showed less sharpness of the maximum point and lower rate of decay than those at low temperatures. The velocity at which the shape of the curves changed increased slightly with increasing temperature.

The data from the method involving rapid changes in crosshead velocity were obtained at the high temperature levels, where enough elongation was displayed, (Figure 12-c).
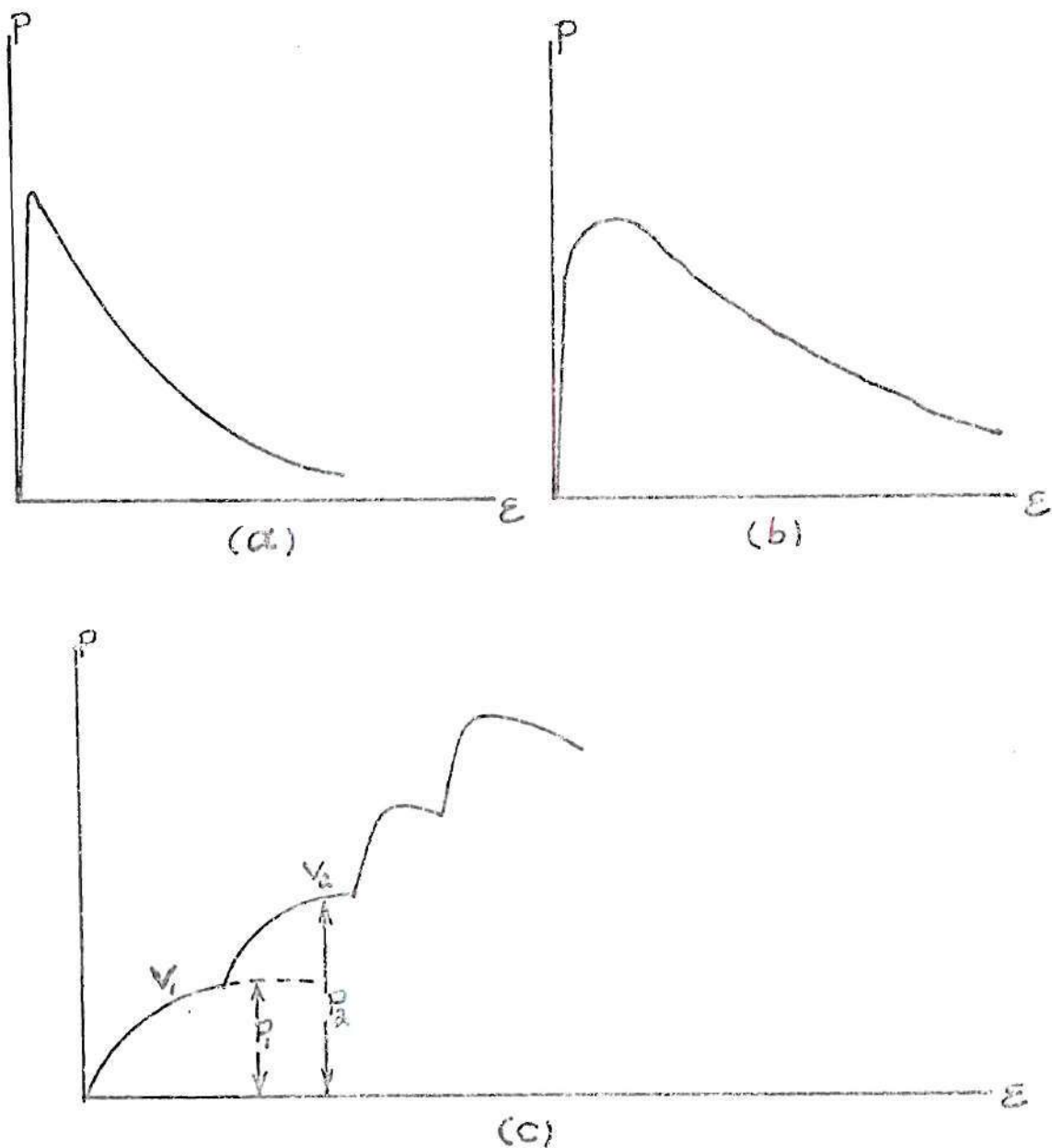
Figure 12. Schematic of Load-Elongation Curves Obtained in
Tensile Testing of Superplastic Al-Zn Alloy.
(a) A sudden rise to a sharp maximum and then
decay, pulled at velocities $V > 1$ in/min and
temperatures lower than about 250°C.   (b) A
sudden rise to a broader maximum and then decay
with a slower rate, pulled at velocities
$V < 1$ in/min and temperatures $T - 250$°C.   (c)
The effect of sudden changes in pulling speed.
The data were obtained at higher temperatures
where enough elongation was displayed.

B. True Stress-True Strain Rate Data

The true stress and true strain rate values were calculated at the point of ultimate load according to the relationships

$$\overline{\sigma} = \frac{P_u}{A_u} \; ; \; \overline{\dot{\varepsilon}} = \frac{V}{\ell_u} \tag{7}$$

where P_u is the maximum load, A_u and ℓ_u are the corresponding cross-sectional area and the specimen length, respectively, and V is the constant crosshead velocity. According to the load-elongation data the true strain rate at the point of maximum load was found to be identical or close to the initial strain rate. Therefore engineering values were employed [28].

The ultimate stress versus initial strain rate is plotted on a log-log scale in Figure 13 at six temperature levels. A family of somewhat S-shaped curves are generated. The shapes of the curves are similar to those of Underwood [25] in tensile tests and Holt [13] in compression tests. For low strain rates the stress is small, then rises gradually with increasing strain rate up to a region where the slope is steepest and the strain rate sensitivity index m is a maximum. The stress then levels off at higher rates.

Considering the variation with temperature, two effects are observed in Figure 13. First, for constant grain size the rate of leveling off is faster at low temperatures
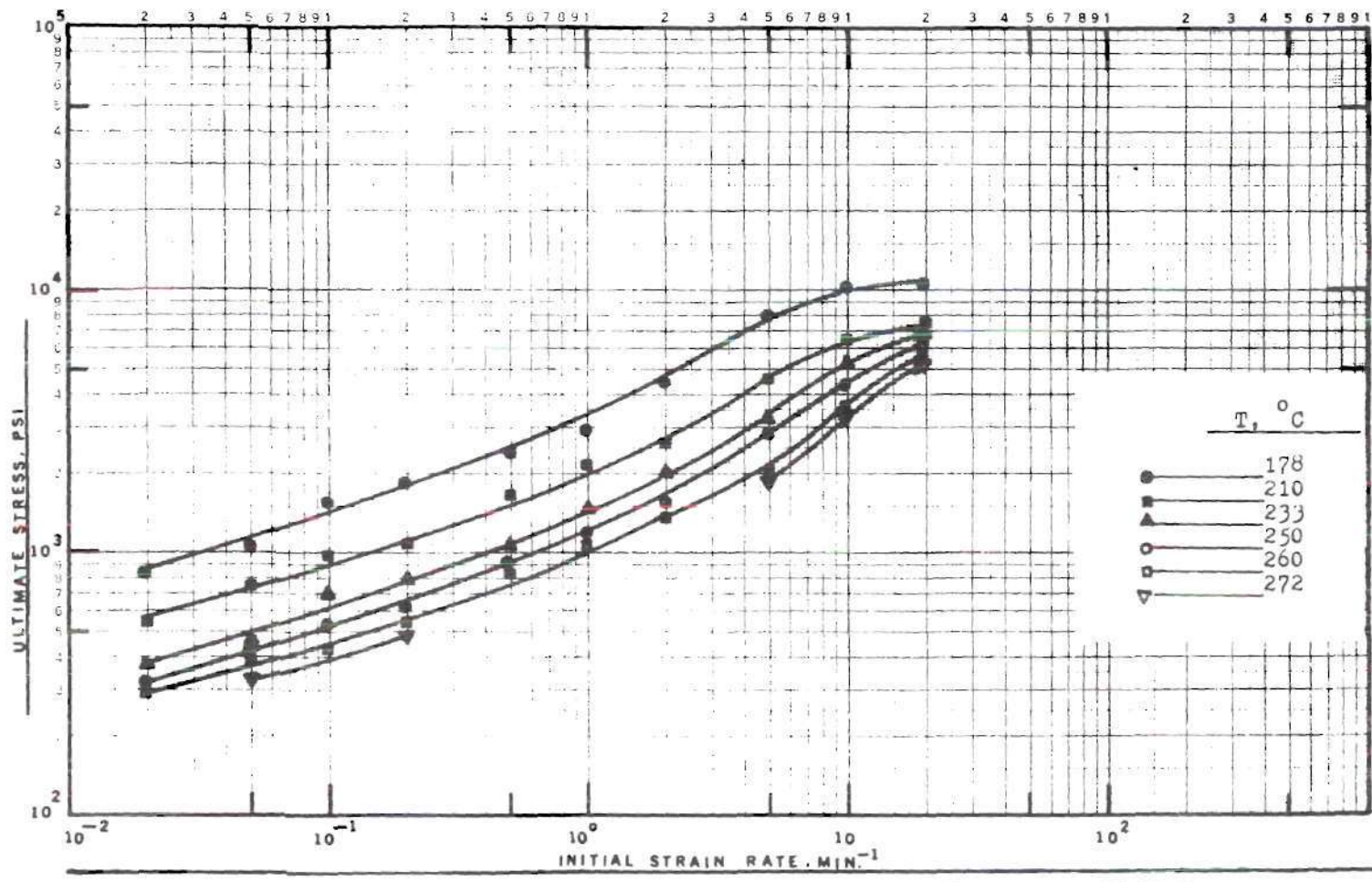
Figure 13. Ultimate Stress Versus Initial Strain Rate for Eutectoid Al-Zn Alloy. Each curve represents different test temperature.

than higher temperatures. This indicates that a slip mechanism comes into play at lower strain rates as temperature is decreased [13,17]. Second, the point of inflection or region of maximum m moves to higher strain rates as the temperature is increased. For example the point of inflection at 178°C lies at about $\dot{\varepsilon} = 1$ min^{-1}, while at 260°C it is shifted to about $\dot{\varepsilon} = 7$ min^{-1}.

A comparison of the curves for two different grain sizes in Figure 14 shows that the fine grained material is weaker than the coarse grained material, at constant strain rate and temperature, as verified frequently in the literature [15,14,13,25]. In addition the region of maximum m is moved to higher strain rates for fine grained material [14, 13,21,25]. Referring to Figure 13 it can be seen that for each curve, the variation of stress as a function of strain rate from the high regime to the intermediate and finally to the low regime, takes place smoothly with no sharp transitions.

C. Strain Rate Sensitivity-Strain Rate Relationship

The slopes of the log stress versus log strain rate curves give the strain rate sensitivity (SRS)

$$m = \frac{\ln \sigma_2 - \ln \sigma_1}{\ln \dot{\varepsilon}_2 - \ln \dot{\varepsilon}_1} \tag{8}$$

assuming a linear relationship between points 1 and 2.
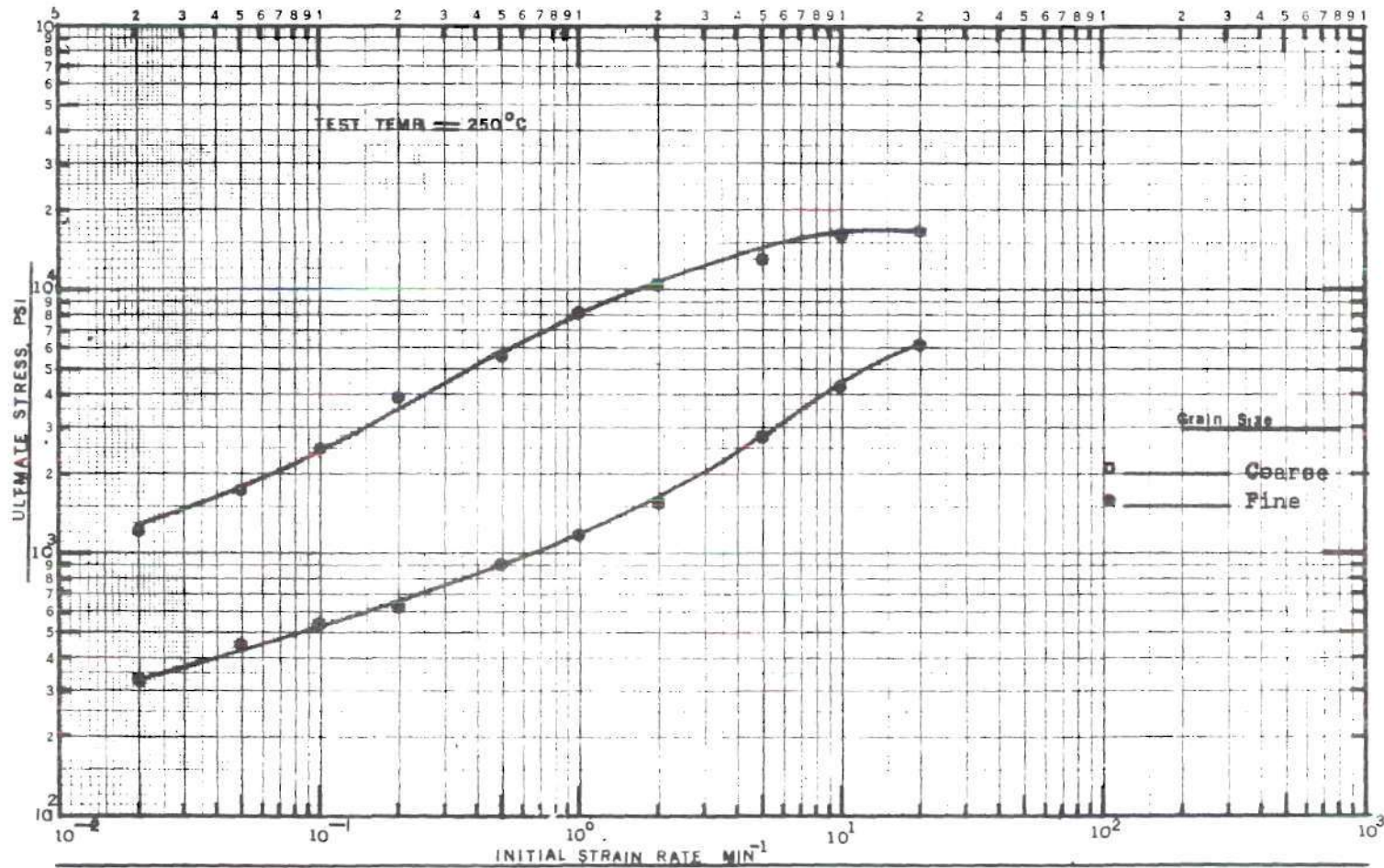
Figure 14. Ultimate Stress Versus Initial Strain Rate for Eutectoid Al-Zn Alloy at 250°C. Each curve represents different grain sizes.

The dependence of SRS upon strain rate and temperature
is shown in Figure 15. The SRS passes through a maximum as
a function of strain rate. This maximum in SRS is shifted
to higher strain rates with increasing temperature. In
addition the maximum m values at higher temperature levels
is greater than at low temperatures. Recalling the prereq-
uisite of $m \geq 0.3$ [15] for superplastic behavior, the curves
reflect the fact that for all test temperatures and strain
rates m falls approximately between 0.3 and 0.7 except for
one point obtained at the lowest temperature and highest
strain rate. The highest m value of 0.7 occurs at the
highest temperature level and strain rate.

The topographic map ($m-\dot{\varepsilon}-T$) of Backofen [12] in
Figure 1 confirms the consistency of the findings in these
experiments. His data cover strain rates up to 1 min^{-1}.
The m curves in his topographic map indicate an extension of
the loop for $m = 0.6$ at strain rates higher than 1 min^{-1}
near the invariant temperature, which was confirmed by the
experiments in this thesis.

The effect of increasing the grain size on rate
sensitivity m is similar to that of lowering the temperature.
For example, Figure 16, which illustrates m versus strain
rate at a constant temperature, for two different grain
sizes, the region of maximum m is shifted toward a lower
strain rate with larger grain size. This result is in general
agreement with the literature [13,14,15,25].
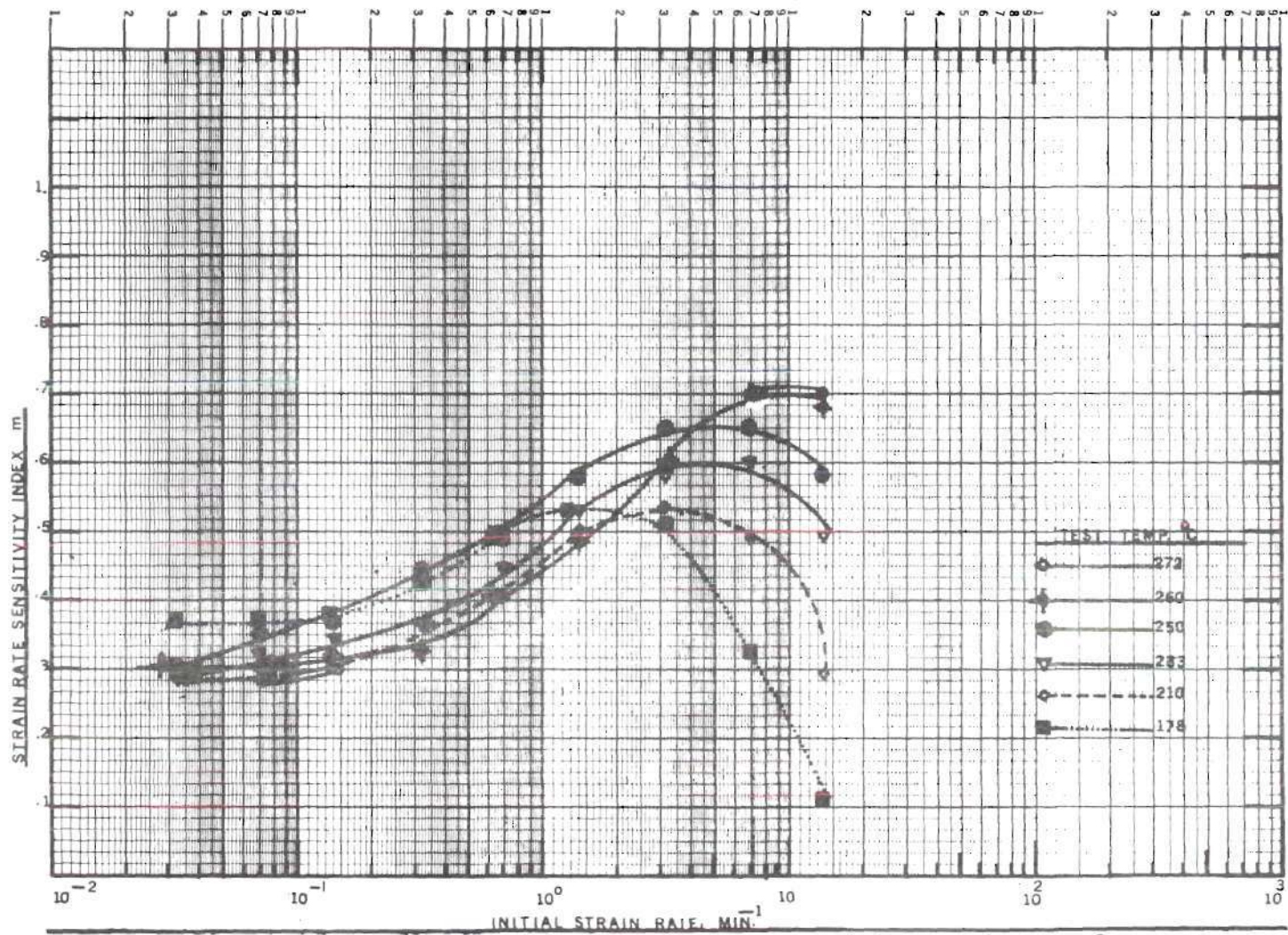
Figure 15. Strain Rate Sensitivity Index m Versus Initial Strain Rate for
Eutectoid Al-Zn Alloy. Each curve represents different test
temperature levels.
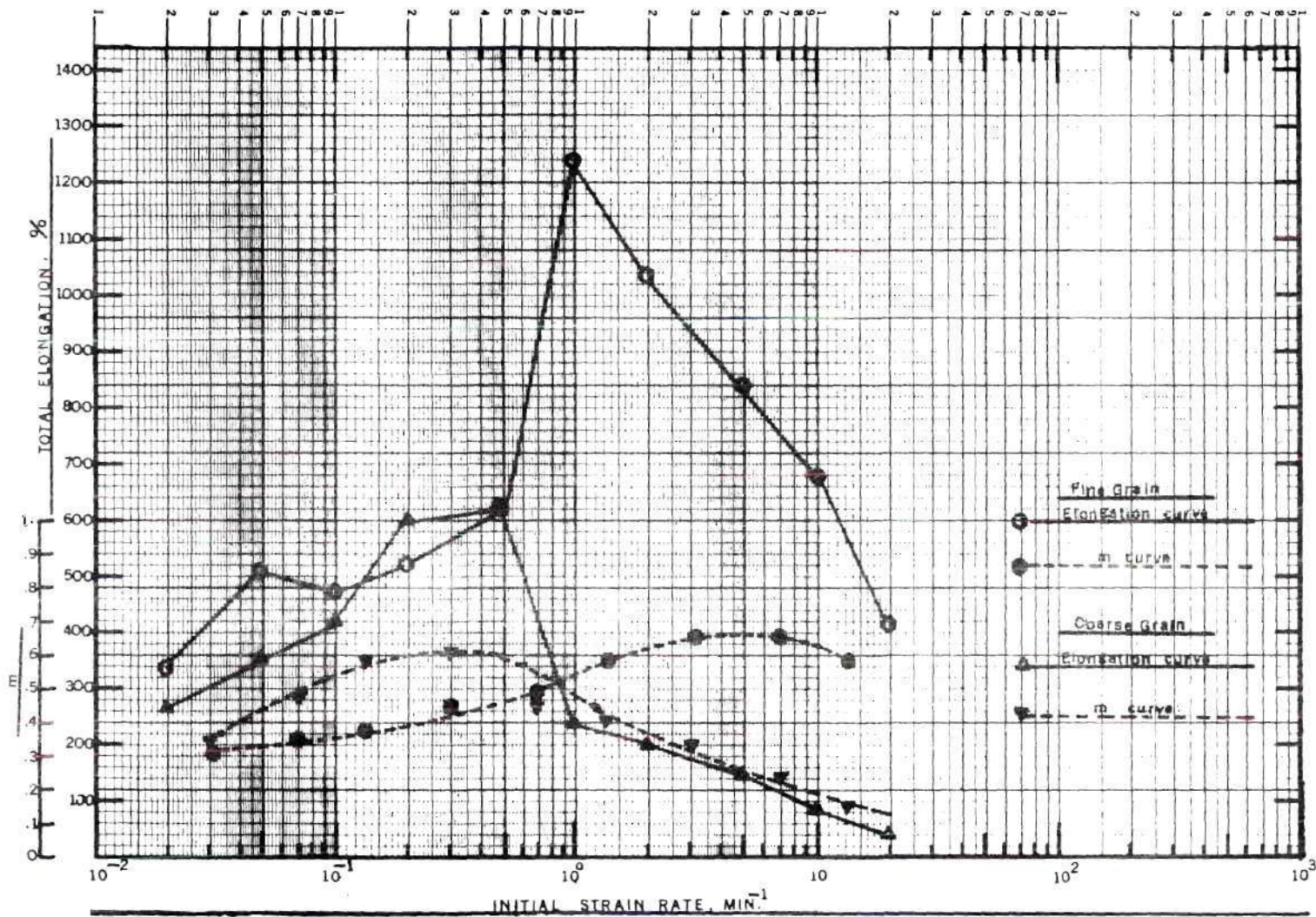
Figure 16. Total Elongation and Strain Rate Sensitivity Index m Versus Initial Strain Rate at 250°C. Each curve represents different grain sizes.

D. Temperature Dependence of Ultimate Stress

Figure 17 illustrates the variation of ultimate tensile stress as a function of temperature and initial strain rates for a constant grain size. The curves are similar to the results of tensile tests of the same material obtained by Underwood [25] and Presnyakov [4]. In this work, curves for ten different strain rates are shown. The variation with temperature has the following effects:

1. At low temperatures the stress is high. It drops drastically with increasing temperature up to the invariant temperature of 275°C.

2. The rate that stress decreases is more rapid at low temperatures than at higher. In other words, as temperature increases, stress becomes less temperature dependent.

3. The stress is less temperature dependent at low strain rates. The curves level off considerably above about 250°C, up to the invariant temperature.

4. The stress begins rising rapidly after the invariant temperature is exceeded. Some data taken at 272°C, which is only three degrees below the invariant, showed a tendency to increase as well.

E. Elongation-Strain Rate Data

In Figure 18 the variation of total elongation is plotted as a function of initial strain rate for different temperature levels. At strain rates equal to or greater than 1 min^{-1}, almost all temperature levels exhibit their
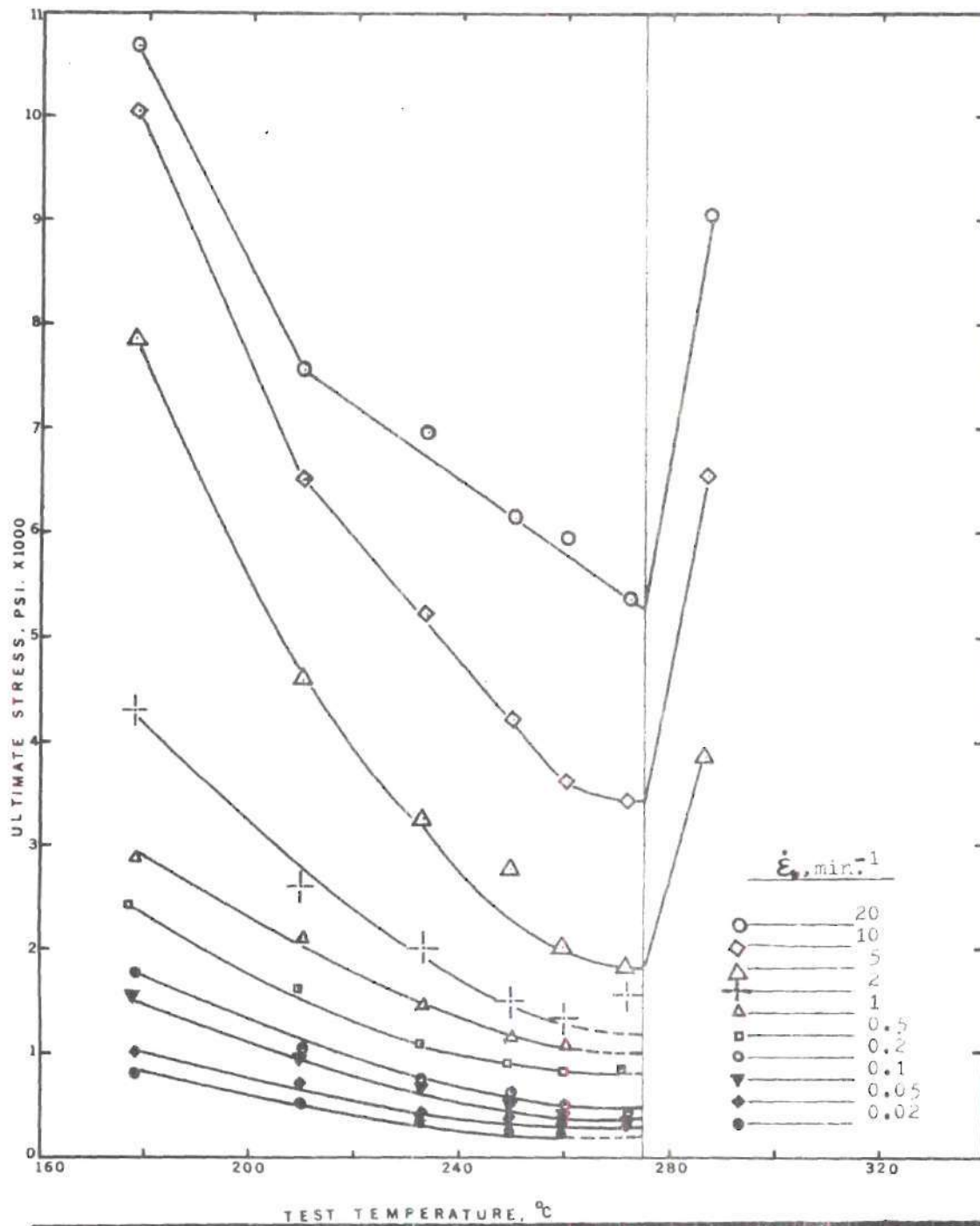
Figure 17. Ultimate Stress Versus Test Temperature for
Al-Zn Eutectoid Alloy. Each curve represents
different strain rates.
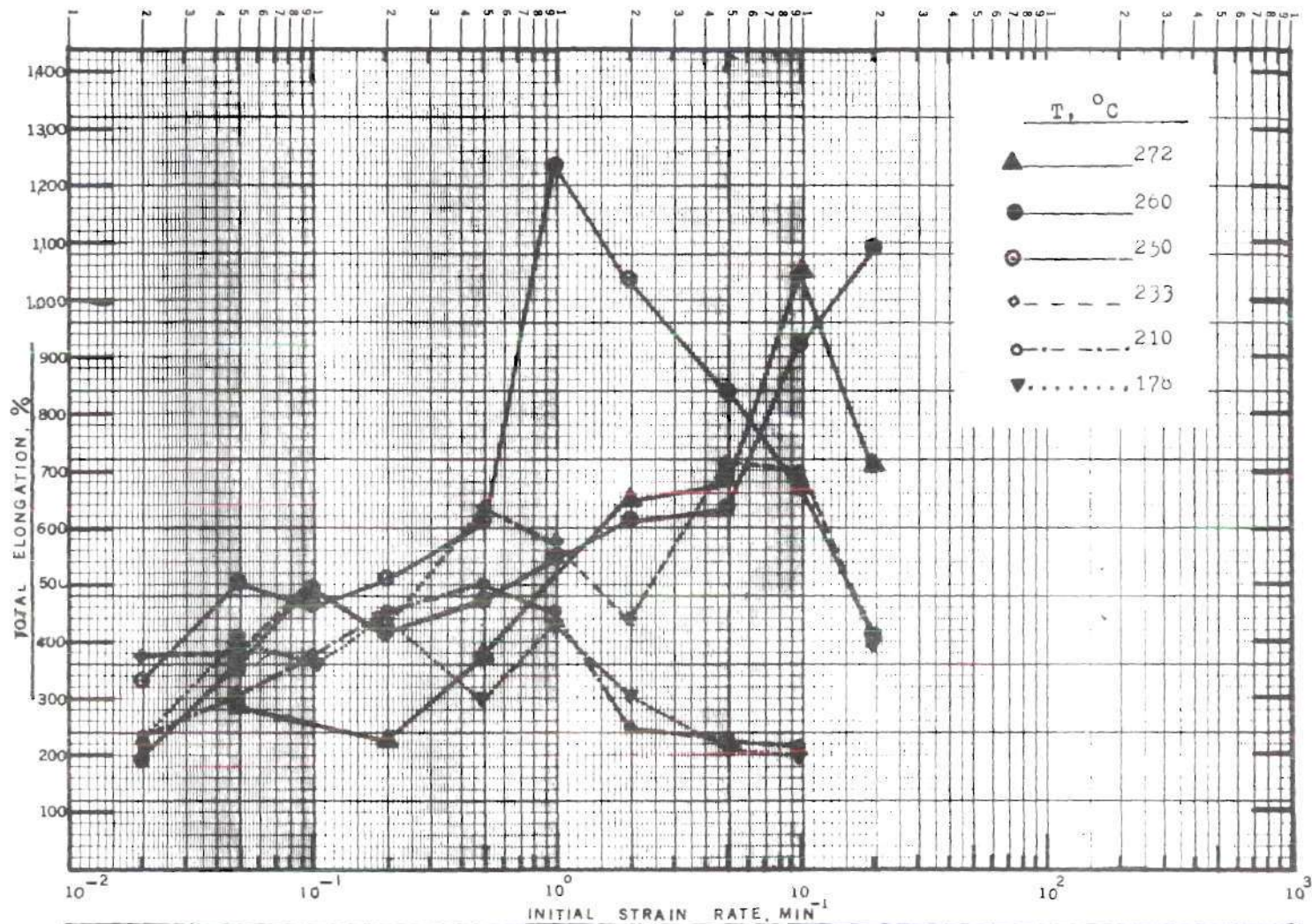
Figure 18. Total Elongation Versus Initial Strain Rate for Al-Zn Eutectoid Alloy. Each curve represents different temperature levels.

maximum extensibility. For example, specimen No. 36, at
$250°C$ and $\dot{\varepsilon} = 1$ min^{-1}, displayed about 1240% elongation. At
this temperature, elongation dropped rapidly at higher or
lower strain rates. For higher test temperatures, the region
of maximum elongation moved toward higher strain rates.
For strain rates less than 0.2 min^{-1} the elongation data
were less systematic.

The degree of consistency of these data can be seen
by comparison with the m versus strain rate curves of Figure
15. Figure 19 gives a cross-plot of total elongation versus
m, taken at corresponding strain rates. The trend of the
data points shows that elongation increases with increasing
m. This result is also found by Backofen, et al. [15].

Referring to Figure 16, the effect of grain size on
the total elongation is illustrated. The maximum m for the
coarse grain size curve corresponds to the region of highest
elongation; however, the correspondence does not obtain for
the fine grain size curves at the temperature.

F. Elongation-Temperature Data

The dependence of total elongation on test temperature
for ten different initial strain rates is illustrated in
Figure 20. The curve representing $\dot{\varepsilon} = 1$ min^{-1} is similar to
the result of Backofen's tensile tests [12]. In general,
for all strain rates the elongation increases with tempera-
tures up to $250°C$. In the region of temperatures higher
than $250°C$, total elongation increases as a function of both
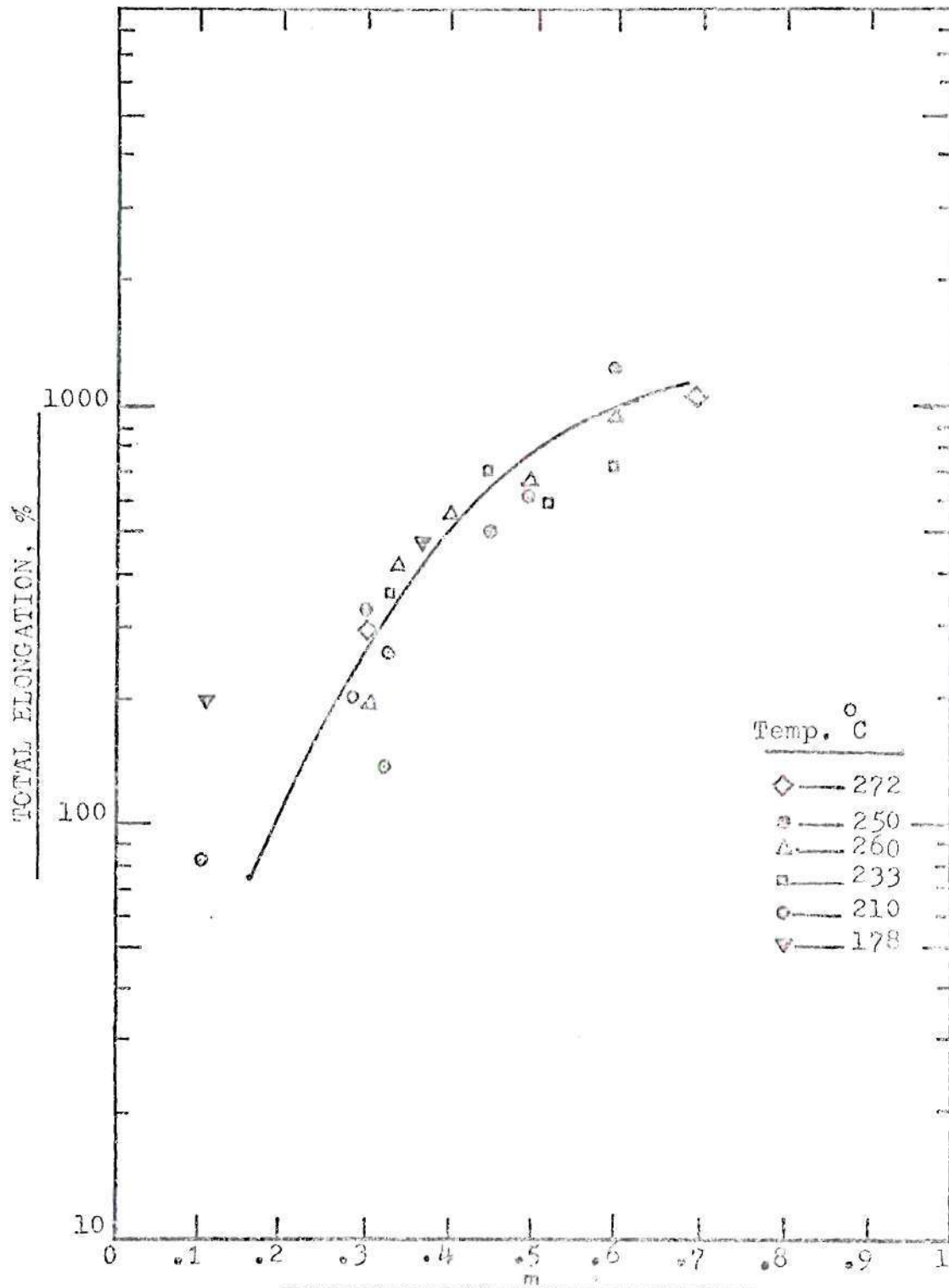
Figure 19. Total Elongation Versus Strain Rate Sensitivity
Index m for Eutectoid Al-Zn Alloy
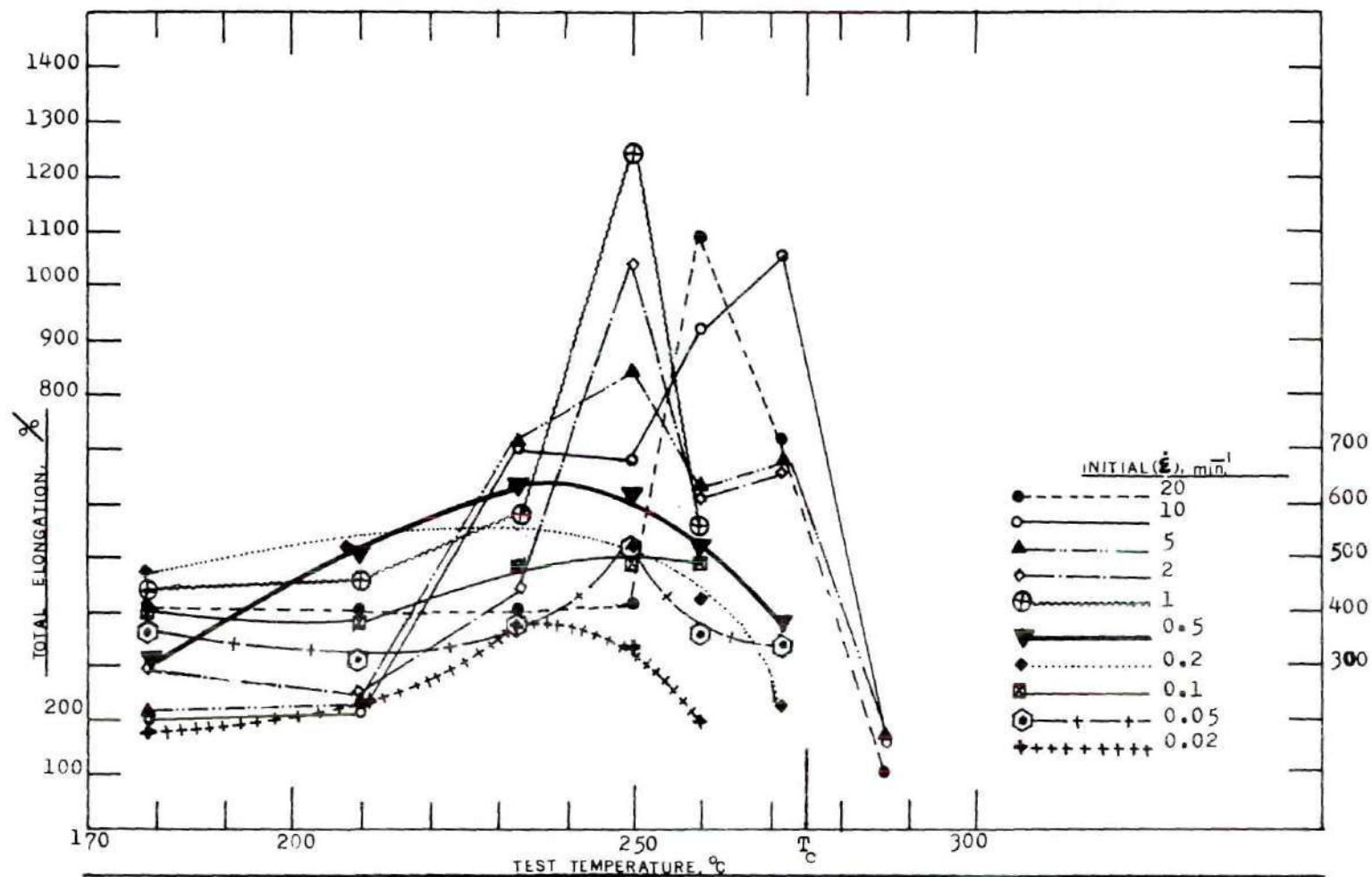
Figure 20. Total Elongation Versus Test Temperature for Al-Zn Eutectoid
Alloy. Each curve represents different strain rates.

strain rate and temperature (only up to the invariant tempera-
ture). Specimens tested in the single phase region at 287°C
did not exhibit any considerable elongation under the
available strain rates from our Instron. According to the
previous literature [12], higher elongations might be
achieved if sufficiently low speed is applied.

G.   Metallography

Metallographic examination was made of the Aℓ-78 wt% Zn
alloy. Upon quenching from the single phase region at 375°C
the alloy decomposes into two phases, finely dispersed
into light-colored aluminum-rich (α) and zinc-rich (β)
regions, as shown in Figure 21-a. If heated again to some
elevated temperature below the invariant and held there to
be aged, the separate phases grow larger and a coarser
structure is formed, Figure 21-b. Grain sizes were measured
by the method of mean intercept length [29,30], giving a
grain size of $\overline{L}_\alpha$ = 0.656 µm for the as-quenched material,
and $\overline{L}_\alpha$ = 1.76 µm for the quenched and aged alloys.

Figures 22-a to 22-f show scanning electron micro-
graphs of the specimens deformed about 400% at six different
temperatures (178, 210, 233, 250, 260 and 272°C), and at a
fixed strain rate of 1 min^{-1}. On the other hand, Figures 23-a
to 23-d show the microstructure of specimens deformed about
400% at a constant temperature of 250°C, but at different
strain rates (0.02, 1, 10 and 20 min^{-1}). From the general
comparison of the grain sizes and grain shapes with respect

(a)
$\overline{L}_\alpha = 0.656$ µm (X5100)
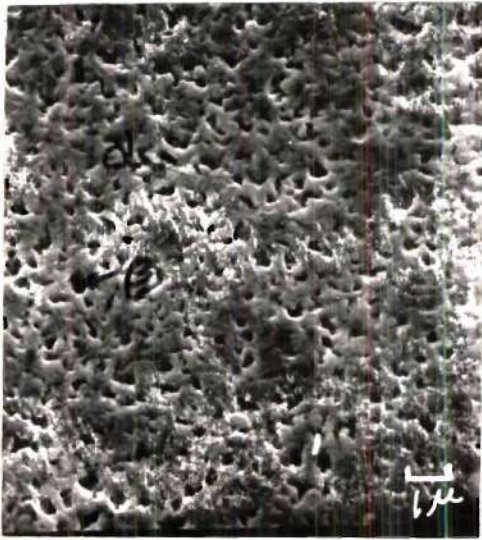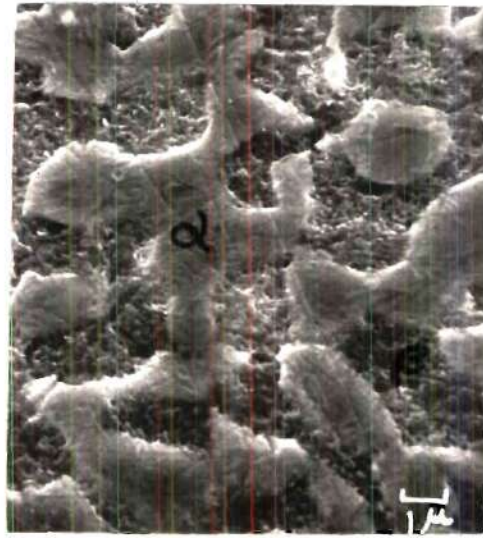
(b)
$\overline{L}_\alpha = 1.76$ µm (X5200)

Figure 21. Microstructures of Al-78 wt % Zn Alloy in
Quenched (a) and Quenched and Aged (b)
Conditions

(a)
$$\frac{T}{\overline{L}_\alpha} = 178\ °C$$
$$= 1.27\ \mu m$$
(X4780)

(b)
$$\frac{T}{\overline{L}_\alpha} = 210°C$$
$$= 1.20\ \mu m$$
(X4850)
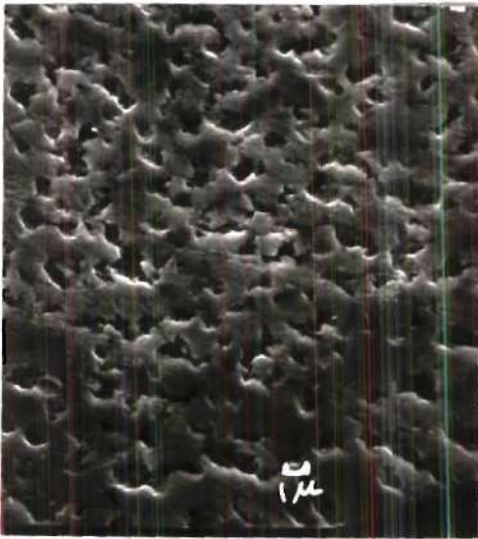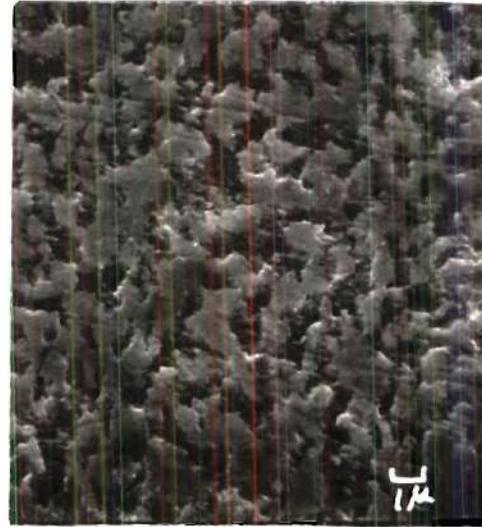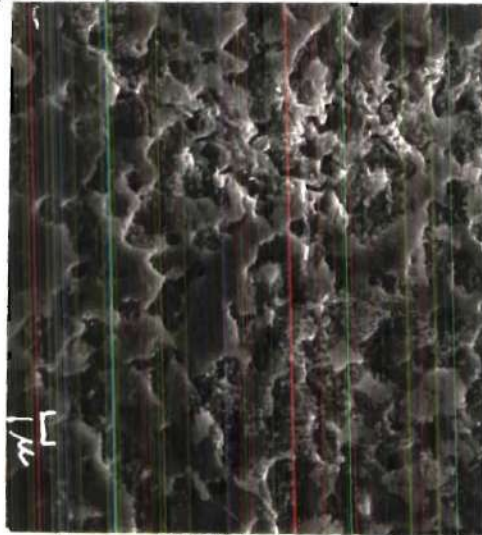
(c) $$\frac{T}{\overline{L}_\alpha} = 233°C$$
$$= 1.205\ \mu m$$
(X4750)

Figure 22.   Microstructures of Al-78 wt. % Zn Alloy, Deformed at a Constant Rate of 1 min^{-1} and Different Temperatures

(d)

$\dfrac{T}{L}_\alpha$ $\begin{array}{l} = 250°C \\ = 1.36 \text{ } \mu m \\ (X4750) \end{array}$
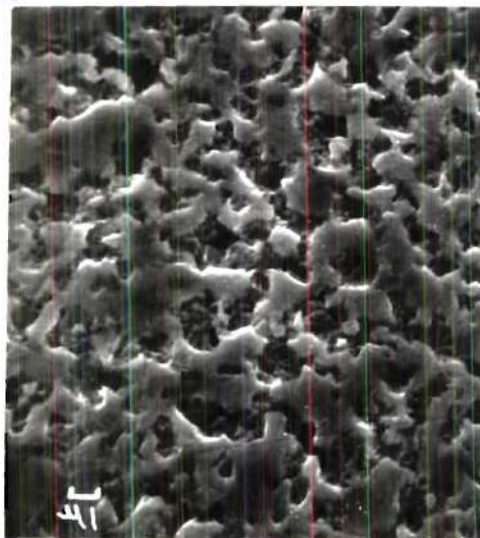
(e)

$\dfrac{T}{L}_\alpha$ $\begin{array}{l} = 260°C \\ = 1.69 \text{ } \mu m \\ (X4780) \end{array}$

(f)

$\dfrac{T}{L}_\alpha$ $\begin{array}{l} = 272°C \\ = 0.92 \text{ } \mu m \\ (X4780) \end{array}$

Figure 22.   (Concluded)

(a)

$\dot{\varepsilon} = 0.02 \text{ min}^{-1}$
$\overline{L}_\alpha = 1.32 \text{ μm}$
(X4800)

(c)

$\dot{\varepsilon} = 10 \text{ min}^{-1}$
$\overline{L}_\alpha = 1.373 \text{ μm}$
(X4800)

(d)
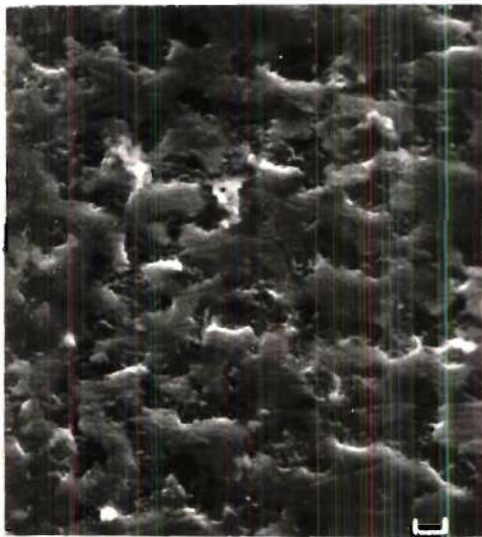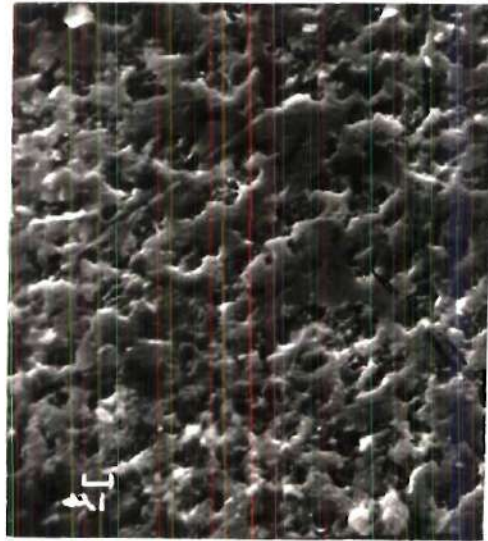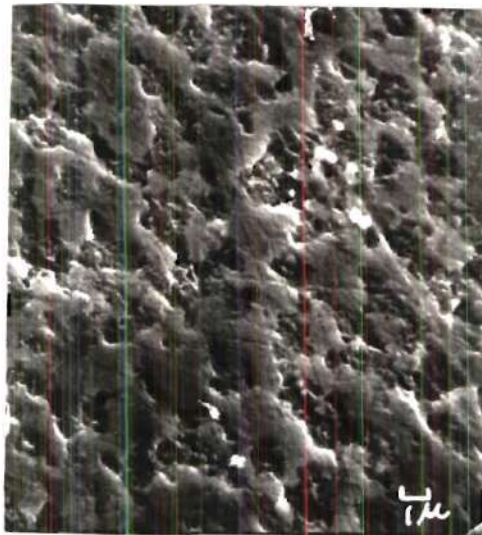
$\dot{\varepsilon} = 20 \text{ min}^{-1}$
$\overline{L}_\alpha = 1.56 \text{ μm}$
(X4750)

Figure 23. Microstructures of Al-78 wt. % Zn Alloy Deformed
           at a Constant Temperature T = 250°C and
           Different Initial Strain Rates. (For Figure
           23-b, see Figure 22-d.)

to the variables T and $\dot{\varepsilon}$, it is apparent that grain size
depends strongly on temperature, while the grain geometry
changes with increased strain rate. The photomicrographs in
Figures 23-c and 23-d indicate some elongation of the grains,
which occurs to a great extent where $\dot{\varepsilon}_O$ is increased

Table 1 summarizes the measured values of grain size
versus T and $\dot{\varepsilon}$. A sample was taken from the grip section of
a specimen deformed at 210°C and 1 min^{-1}, and its micro-
structure is shown in Figure 24. $\overline{L}_\alpha$ for the grip section
was found to be 1.02 μm. The original grain size in the
quenched condition was $\overline{L}_\alpha$ = 0.656 μm. Thus there was about
a 50 percent increase in grain size between the original
grain size and the grain size in the grip section. This
increase came about during the preliminary 35 minutes holding
time in the furnace before the test started. From Table 1
at 210°C and 1 min^{-1}, we see that a sample from the specimen
gage length had $\overline{L}_\alpha$ = 1.20 μm. This represents about a 20
percent increase in grain size between the grip and deformed
section. Thus the grain size remained in the superplastic
range, even though there was some slight, unavoidable
increase during superplastic deformation.

$$\frac{T}{L}_\alpha \begin{array}{l} = 210°C \\ = 1.02 \ \mu m \ (X5400) \end{array}$$
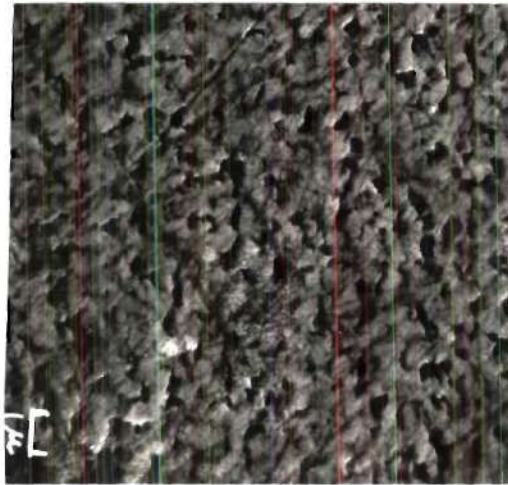
Figure 24.   Microstructure of Al-78 wt. % Zn Alloy from a
Specimen Grip Section. (Pulled at 210°C and
a Strain Rate of 1 min^{-1}.)

Table 1. Mean Intercept Lengths (a) of Selected Specimens

Temperature (°C)	Strain Rates (min^{-1})			
	0.02	1.0 (b)	10.0	20.0
272		(0.92)		
260		1.69		
250 (c)	1.32	1.36	1.27	1.56
233		1.20		
210		1.20		
178		1.27		

(a) Mean intercept length, $\overline{L}_\alpha = \dfrac{(V_V)\alpha}{(P_L)\alpha\beta}$, μm. where α is light colored phase. (See Figure 21-a and 21-b.)

(b) Photomicrographs appear in Figures 22.

(c) Photomicrographs appear in Figures 23.

CHAPTER V

DISCUSSION AND CONCLUSIONS

Experiments performed in this thesis have centered on the mechanical properties of superplastic Al-78 wt % Zn alloy at and around the transition region between the high stress and low stress regimes. This transition state has been identified with maximum superplastic properties [12,13, 14,19], in which grain boundary sliding becomes dominant. Detailed studies have revealed that the occurrence of GBS can be linked to high m values, large elongations under low stress and only slight microstructural changes evident after deformation.

Variation of test temperature and rate of deformation are the two main parameters with which to study super-plasticity in an alloy (provided that the grain size is fixed). In these experiments a temperature range of about 100°C and a strain rate range of about three orders of magnitude have been employed. The evidence we have obtained here bearing on the type of transition behavior that occurs during superplastic deformation, is as follows:

1. The curves of m versus $\dot{\varepsilon}$ in Figure 15 show that m exceeds 0.3 over almost all of the strain rate range. Between the maximum values of m and the fall-offs to either

side, there are gradual changes without any indication of sharp breaks. This is seen to be so for all test temperatures.

2. The variation of ultimate stress with strain rate is described by the curves in Figure 13. The regions within which the points of inflection lie (maximum m) are identified as the GBS dominant regions [13,14,16,17,19]. Transition from those regions to the high stress levels where slip occurs [13,14,17,19] or to the lower stresses where N-H creep is the predominant mechanism [16,17], follows a smooth path rather than passing through a sharp point. The point of inflection moves toward the higher strain rates and the steepness of the curve at this point increases as the test temperature is increased. This indicates that the GBS region becomes wider with increasing temperature.

3. An analysis of the temperature dependence of stress reflects much the same picture as with strain rates. That is, the transition from high to low stress levels with temperature is a gradual process, at least, at the lower strain rates. Figure 17 illustrates that at low temperature, where stress is high, there is little evidence of sharp transitions into the low stress (high temperature) region. Moreover, as the temperature increases, stress becomes less temperature dependent. This effect is attributed to the contribution of fluctuations, enhanced by an increased temperature. Once the short range barriers in a stress field

are governed by thermal fluctuations, further increases in
temperature would have less effect on lowering the stress
[31]. For the two highest strain rates in Figure 17, the
curves through the available data points go through a some-
what sharper point. These could be considered a sharp
transition. This effect agrees somewhat with Ashby's
argument [19], that for large strains the intermediate regime
(see Figure 5) becomes narrower, because of the dislocation-
creep component interfering with GBS. For our case, shown
in Figure 17, the regime in question corresponds to a
larger dislocation creep contribution, which would be expected
as we get farther from the superplastic region.

 4. From Figures 18 and 20 the dependence of total
elongation on the strain rate and temperature can be analyzed.
From both types of curves we see that total elongations of
more than 500% are achieved within an order of magnitude
range of strain rates and a 30°C temperature range in the
vicinity of 250°C. Cross plots of maximum elongations versus
their temperatures and strain rates, reveal smoothly varying
curves with again no apparent sharp breaks in the inter-
mediate regions. Thus the maximum elongation data do not
indicate a sharp transition.

 5. For the best correlation between the mechanical
properties and the microstructure, many more micrographs of
all the specimens tested are essential. Unfortunately the
magnifications required for resolving the very fine grain

size require extensive use of the electron microscope. Scanning electron micrographs were taken from selected samples showing a gradual trend of microstructural changes with both temperature and strain rates. Thus, here too the results showed no sharp transition from the microstructural point of view.

6. In Figure 25 we plot log $\dot{\varepsilon}$ (at a stress of 2000 psi) vs 1/T, obtaining six points that fall fairly close to a straight line, the slope of which is about 14,200 cal/mol. This value can be considered an activation energy for the superplastic deformation process, since the data points were obtained from the central region of the curves in Figure 13. This value is in accord with 14,500 cal/mol reported for the eutectoid Al-Zn alloy by Davies, et al. [22]. From the value of activation energy for grain boundary diffusion of zinc of 14,000 cal/mol [22] it may be possible to identify the deformation process studied here with grain boundary diffusion of zinc. Further research is needed to clarify this point, however.

Again no discontinuities are observed, adding additional credence to the other data showing smooth, gradual curves in the superplastic range of variables.

7. Another way of analyzing the data is presented in Figure 26. A combined temperature-strain rate parameter is used [32] to consolidate all the ultimate stress data into one curve. The constant C = 7 is obtained directly from the
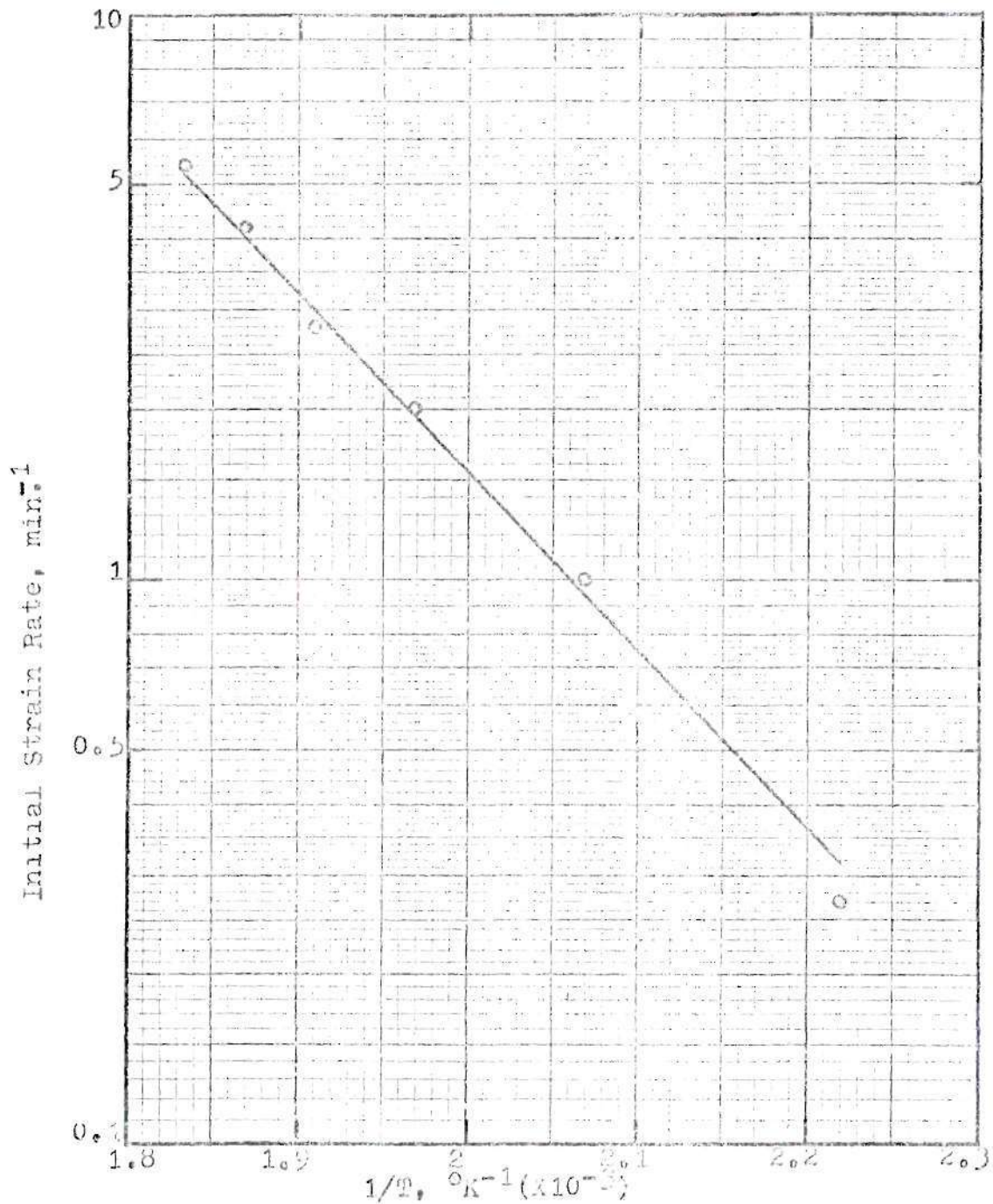
Figure 25. $\dot{\varepsilon}_0$ Versus 1/T is Plotted at a Constant Ultimate Stress (2000 psi). (The slope of the curve represents the superplastic activation energy, equivalent to 14200 cal/mol.)
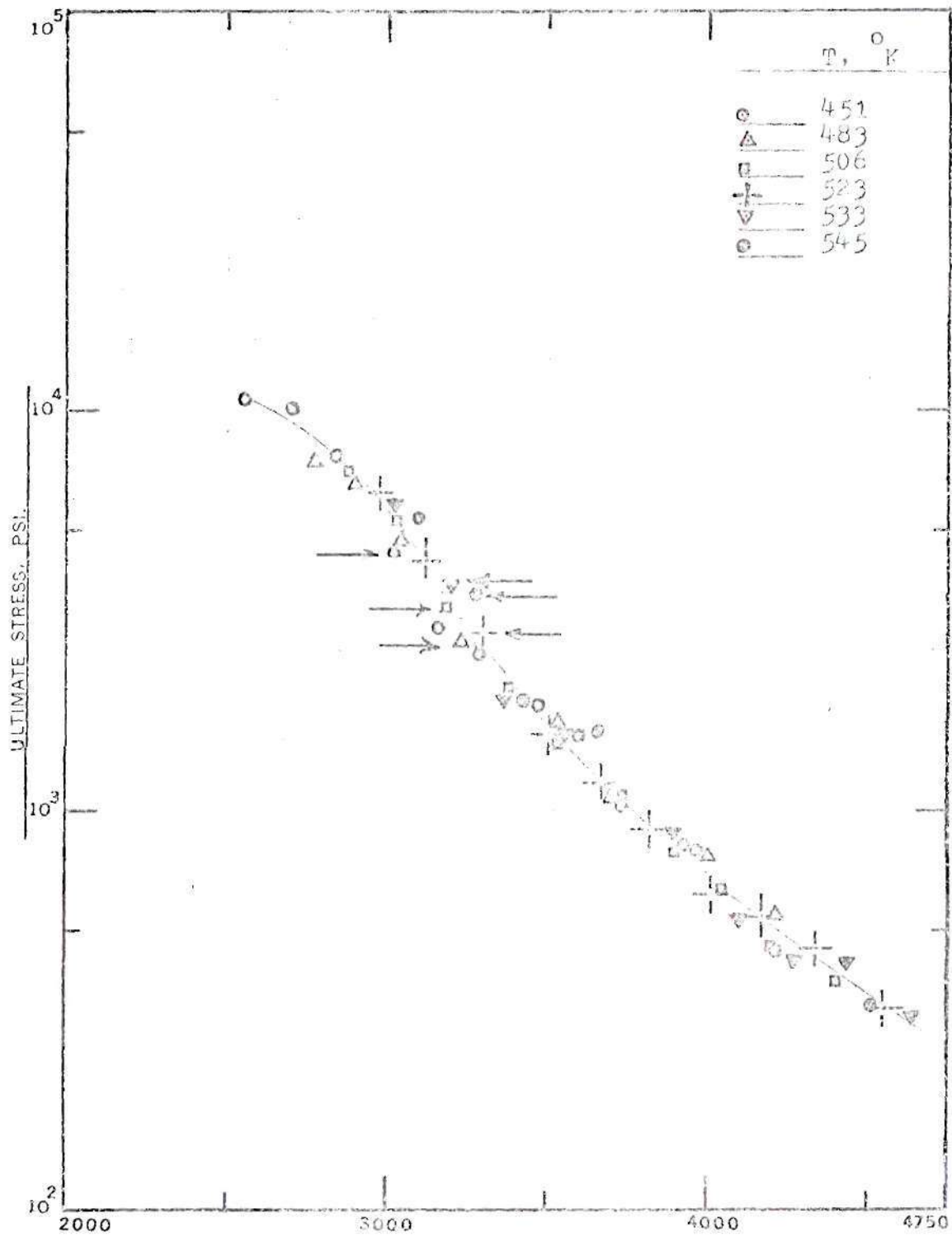
Figure 26. Ultimate Stress Versus the Combined Parameter of T and $\dot{\varepsilon}_o$. (The arrows indicate locations of max m-values.)

original curves at a selected stress level by solution of the equation:

$$T_1(C-\log\dot{\varepsilon}_1) = T_2(C-\log\dot{\varepsilon}_2) \qquad (9)$$

Using this method of analysis, we see that for each stress there is only one parameter value, which is a constant for that stress. T and $\dot{\varepsilon}$ can vary, however, provided the parameter value remains constant. Moreover, if T is held constant, we have, in effect, a stress versus negative log $\dot{\varepsilon}$ plot, which can be compared readily with the conventional plot of log stress versus log strain rate.

The important feature of this plot of σ_u versus the parameter is that no sharp discontinuities are apparent. There is only a smoothly varying curve between the high stress region and the low stress region.

The location of the points corresponding to the maximum m values (from Figure 15) are marked in Figure 26 by arrows. It can be seen that they lie within the region where diffusion-accommodated flow is dominant, identified by Ashby as low stress regime [19] (see Figure 5). The locus of points from this regime to the intermediate and then to higher stress regimes follows a gradual rising path. By combining all data by means of a parameter plot we have additional confirmation of the original log σ_u versus log $\dot{\varepsilon}$ plots, i.e., that the transition region is essentially a

smooth and not a sharp one.

The fact that the maximum m-values conform to this combined plot implies that they can be obtained by suitable combinations of T and $\dot{\epsilon}$. This may be taken as further confirmation that the transition from the region of optimum superplasticity occurs gradually over a range of variables.

We conclude, therefore, under the conditions studied here, for the alloy selected, and initial microstructural state, that the superplastic region is not identifiable as a sharp transition region. Thus, it appears that a gradual merging of high and low stress regimes into the region of maximum superplasticity effect is the operative process in this case.

Table 2-a. Experimental and Calculated Data for
Fine Grain Size Material.
Test Temperature = 178°C.

$\ell_o = 1.0$ in.
$A_o = 9.1647 \times 10^{-3}$ in^2

Spec No.	Initial Velocity V_o (in/min)	Ultimate Load P_u (lbs)		Strain at Point P_u (in/in)	True Strain Rate $\dot{\varepsilon}_o$ (min^{-1})	True Stress $\bar{\sigma}_u$ (psi)	SRS Index m	Total Elongation %
1	0.02	7.4	7.4	0.08	0.02	807.4	0.364	188
2	0.05	9.4	9.4	0.09	0.05	1025	0.364	363
3	0.1	14.3	14.3	0.05	0.1	1560	0.364	400
4	0.2	16.8	16.8	0.06	0.2	1833	0.425	469
5	0.5	26.5 18	22.2	0.08	0.5	2422	0.488	125 300
6	1	26.3	26.3	0.03	1	2869	0.51	413
7	2	31.3 48.2	39.75	0.04	2	4337	0.51	506 300
8	5	72	72	0.04	5	7856	0.325	213
9	10	92	92	0.03	10	10038	0.11	200
10	20	98	98	0.04	20	10693		413

Table 2-b. Experimental and Calculated Data for
Fine Grain Size Material.
Test Temperature = 210°C.

ℓ_o = 1.0 in.
A_o = 9.1647x10^{-3}in^2

Spec. No.	Initial Velocity V_o (in/min)	Ultimate Load P_u (lbs)		Strain at Point P_u (in/in)	True Strain Rate $\dot{\bar{\varepsilon}}_o$ (min^{-1})	True Stress $\bar{\sigma}_u$ (psi)	SRS Index m	Total Elongation %
11	0.02	4.1 / 4.9	4.9	0.06	0.02	534.6	0.306	325 / 225
12	0.05	8.4 / 6.8	6.8	0.04	0.05	741.9	0.306	not pulled to fracture / 300
13	0.1	9 / 9.6	9	0.03	0.01	981.9	0.306	325 / 375
14	0.2	9.6	9.6	0.02	0.2	1048	0.364	450
15	0.5	14.8	14.8	0.05	0.5	10615	0.404	500
16	1	19.5	19.5	0.04	1	2128	0.51	450
17	2	24	24	0.03	2	2619	0.532	244
18	5	42	42	0.04	5	4583	0.488	225
19	10	60	60	0.01	10	6547	0.286	213
20	20	69.5	69.5	0.02	20	7583		400

Table 2-c. Experimental and Calculated Data for Fine Grain Size Material. Test Temperature = 233°C.

$\ell_o = 1.0$ in.
$A_o = 9.1647 \times 10^{-3} in^2$

Spec. No.	Initial Velocity V_o (in/min)	Ultimate Load P_u (lbs)		Strain at Point P_u (in/in)	True Strain Rate $\dot{\bar{\varepsilon}}_o$ (min⁻¹)	True Stress $\bar{\sigma}_u$ (psi)	SRS Index m	Total Elongation %
21	0.02	3.4	3.4	0.1	0.02	371	0.306	375
22	0.05	4.2	4.2	0.07	0.05	458.3	0.325	363
23	0.1	6.35	6.35	0.06	0.1	629.9	0.344	475
24	0.2	7.2	7.2	0.04	0.2	785.6	0.364	375
25	0.5	8.9 11	10	0.04	0.5	1091	0.446	625 450
26	1	15.4 13.6	13.6	0.03	1	1484	0.532	463 575
27	2	15.7 18.5	18.5	0.02	2	2019	0.578	400 430
28	5	29.8 30	29.9	0.05	5	3262	0.601	710 525
29	10	43.5 48	48	0.04	10	5237	0.446	700 431
30	20	63.8 64.5	64.15	0.03	20	6999		387 400

Table 2-d. Experimental and Calculated Data for
Fine Grain Size Material.
Test Temperature = 250°C.

ℓ_o = 1.0 in.
A_o = 9.1647x10^{-3}in^2

Spec. No.	Initial Velocity V_o (in/min)	Ultimate Load P_u (lbs)		Strain at Point P_u (in/in)	True Strain Rate $\bar{\dot{\varepsilon}}_o$ (min^{-1})	True Stress $\bar{\sigma}_u$ (psi)	SRS Index m	Total Elongation %
31	0.02	3	3	0.1	0.02	327	0.306	335
32	0.05	4.1	4.1	0.1	0.05	447	0.346	506
33	0.1	5.84	4.9	0.08	0.1	535	0.364	463 500
34	0.2	5.6 4.4	5.6	0.05	0.2	612	0.446	513 375
35	0.5	8.5 8	8.25	0.06	0.5	900	0.488	375 613
36	1	13.25 8	10.7	0.05	1	1168	0.578	566 1238
37	2	14	14	0.02	2	1528	0.65	1038
38	5	32.5 25.5	25.5	0.03	5	2782	0.65	488 838
39	10	38.8	38	0.04	10	4233	0.578	675
40	20	56.5	56.5	0.02	20	6165		413

Table 2-e. Experimental and Calculated Data for
Fine Grain Size Material.
Test Temperature = 260°C.

ℓ_o = 1.0 in.
A_o = 9.1647x10^{-3} in^2

Spec. No.	Initial Velocity V_o (in/min)	Ultimate Load P_u (lbs)		Strain at Point P_u (in/in)	True Strain Rate $\dot{\bar{\varepsilon}}_o$ (min^{-1})	True Stress $\bar{\sigma}_u$ (psi)	SRS Index m	Total Elongation %
41	0.02	2.8	2.8	0.04	0.02	306	0.06	188
42	0.05	3.8	3.8	0.05	0.05	415	0.306	350
43	0.1	3.8	3.8	0.05	0.1	415	0.325	490
44	0.2	4.8	4.8	0.03	0.2	524	0.325	419
45	0.5	8.1 8	8.05	0.04	0.5	878	0.404	580 475
46	1	9.8 10	9.9	0.07	1	1080	0.488	550 525
47	2	12.5 16	14.25	0.06	2	1555	0.606	475 613
48	5	17.8 18.5	18.1	0.03	5	1975	0.7	630 538
49	10	34.4 32.2	33.3	0.04	10	3633	0.675	825 919
50	20	55 54.7	54.9	0.02	20	5990		838 1088

Table 2-f. Experimental and Calculated Data for
Fine Grain Size Material.
Test Temperature = 272°C.

$\ell_o = 1.0$ in.
$A_o = 9.1647 \times 10^{-3} \text{in}^2$

Spec. No.	Initial Velocity V_o (in/min)	Ultimate Load P_u (lbs)		Strain at Point P_u (in/in)	True Strain Rate $\dot{\varepsilon}_o$ (min^{-1})	True Stress $\bar{\sigma}_u$ (psi)	SRS Index m	Total Elongation %
51	0.02				0.02			
52	0.05	3.1	3.1	0.06	0.05	338	0.286	285
53	0.1				0.1			
54	0.2	4.1	4.1	0.05	0.2	447	0.306	225
55	0.5	7.3	7.3	0.04	0.5	797		375
56	1				1			
57	2	14.5	14.5	0.07	2	1582		650
58	5	16.8	16.8	0.05	5	1833	0.7	675
59	10	31.5	31.5	0.05	10	3437	0.7	1050
60	20	49.5	49.5	0.02	20	5400		710

Table 2-g. Experimental and Calculated Data for
Coarse Grain Size Material.
Test Temperature = 250°C.

ℓ_o = 1.0 in.
A_o = 9.1647x10^{-3}in^2

Spec. No.	Initial Velocity V_o (in/min)	Ultimate Load P_u (lbs)	Strain at Point P_u (in/in)	True Strain Rate $\dot{\bar{\varepsilon}}_o$ (min^{-1})	True Stress $\bar{\sigma}_u$ (psi)	SRS Index m	Total Elongation %
71	0.02	11	0.04	0.02	1200	0.325	262
72	0.05	15.7	0.05	0.05	1713	0.467	350
73	0.1	22.7	0.05	0.01	2477	0.578	413
74	0.2	35	0.04	0.2	3819	0.602	600
75	0.5	50.5	0.05	0.5	5510	0.467	619
76	1	73.5	0.07	1	8020	0.404	238
77	2	94	0.05	2	10256	0.325	200
78	5	118	0.04	5	12875	0.213	150
79	10	146	0.04	10	15930	0.105	81
80	20	150	0.03	20	16366		38

Table 3-a. Experimental and Calculated Data
on the Parameter
$\P = T(C-\log \dot{\epsilon}_O)$

Test Temperature = 451°K   C = 7

$\dot{\epsilon}_O$ (min^{-1})	$\log \dot{\epsilon}_O$	$(C-\log \dot{\epsilon}_O)$	$T(C-\log \dot{\epsilon}_O)$	σ_u (psi)
0.02	-1.699	8.699	3923	807
0.05	-1.301	8.301	3744	1026
0.1	-1	8	3608	1560
0.2	-0.699	7.699	3472	1833
0.5	-0.301	7.301	3293	2422
1	0	7	3157	2870
2	0.301	6.699	3021	4337
5	0.699	6.301	2841	7856
10	1	6	2706	10038
20	1.301	5.699	2570	10693

Table 3-b.   Experimental and Calculated Data
on the Parameter
$\P = T(C-\log \dot\varepsilon_o)$

Test Temperature = 483°K   C = 7

$\dot\varepsilon_o$ (min^{-1})	$\log \dot\varepsilon_o$	$(C-\log \dot\varepsilon_o)$	$T(C-\log \dot\varepsilon_o)$	σ_u (psi)
0.02	-1.699	8.699	4201	535
0.05	-1.301	8.301	4009	742
0.1	-1	8	3864	981
0.2	-0.699	7.699	3718	1048
0.5	-0.301	7.301	3526	1615
1	0	7	3381	2128
2	0.301	6.699	3236	2619
5	0.699	6.301	3042	4583
10	1	6	2898	6547
20	1.301	5.699	2753	7583

71

Table 3-c. Experimental and Calculated Data
on the Parameter
$\P = T(C-\log \dot{\varepsilon}_o)$

Test Temperature = 506°K   C = 7

$\dot{\varepsilon}_o$ (min^{-1})	$\log \dot{\varepsilon}_o$	$(C-\log \dot{\varepsilon}_o)$	$T(c-\log \dot{\varepsilon}_o)$	σ_u (psi)
0.02	-1.699	8.699	4401	371
0.05	-1.301	8.301	4200	458
0.1	-1	8	4048	630
0.2	-0.699	7.699	3895	786
0.5	-0.301	7.301	3694	1091
1	0	7	3542	1484
2	0.301	6.699	3390	2019
5	0.699	6.301	3188	3262
10	1	6	3036	5237
20	1.301	5.699	2883	6999

Table 3-d. Experimental and Calculated Data
on the Parameter
$\P = T(C-\log \dot{\varepsilon}_o)$

Test Temperature = 523°K   C = 7

$\dot{\varepsilon}_o$ (min^{-1})	$\log \dot{\varepsilon}_o$	$(C-\log \dot{\varepsilon}_o)$	$T(C-\log \dot{\varepsilon}_o)$	σ_u (psi)
0.02	-1.699	8.699	4550	327
0.05	-1.301	8.301	4341	447
0.1	-1	8	4184	535
0.2	-0.699	7.699	4027	612
0.5	-0.301	7.301	3818	900
1	0	7	3661	1168
2	0.301	6.699	3504	1528
5	0.699	6.301	3295	2782
10	1	6	3138	4233
20	1.301	5.699	2981	6165

Table 3-e. Experimental and Calculated Data
on the Parameter
$\P = T(C-\log \dot\varepsilon_o)$

$\dot\varepsilon_o$ (min^{-1})	$\log \dot\varepsilon_o$	$(C-\log \dot\varepsilon_o)$	$T(C-\log \dot\varepsilon_o)$	σ_u (psi)
0.02	-1.699	8.699	4636	306
0.05	-1.301	8.301	4424	415
0.1	-1	8	4264	415
0.2	-0.699	7.699	4103	524
0.5	-0.301	7.301	3891	878
1	0	7	3731	1080
2	0.301	6.699	3570	1555
5	0.699	6.301	3358	1975
10	1	6	3198	3633
20	1.301	5.699	3037	5990

T = 533°K   C = 7

Table 3-f. Experimental and Calculated Data
on the Parameter
$\P = T(C-\log \dot{\varepsilon}_o)$

Test Temperature = 545°K   C = 7

$\dot{\varepsilon}_o$ (min^{-1})	$\log \dot{\varepsilon}_o$	$(C-\log \dot{\varepsilon}_o)$	$T(C-\log \dot{\varepsilon}_o)$	σ_u (psi)
0.02	-1.699	8.699	4741	
0.05	-1.301	8.301	4520	338
0.1	-1	8	4360	
0.2	-0.699	7.699	4195	447
0.5	-0.301	7.301	3979	797
1	0	7	3815	
2	0.301	6.699	3651	1582
5	0.699	6.301	3434	1833
10	1	6	3270	3437
20	1.301	5.699	3106	5400

Table 4. Calculation of C from the Relationship
$$T_1(C-\log \dot{\epsilon}_1) = T_2(C-\log \dot{\epsilon}_2)$$

$T(°C)$	$T(°K)$	$\sigma_u(psi)$	$\dot{\epsilon}_o(min^{-1})$	$\log \dot{\epsilon}(min^{-1})$
194	467	2000	0.5	-0.301
210	483	2128	1	0
233	506	2018	2	0.301
260	533	1975	5	0.699

$$C = \log \frac{\dot{\epsilon}_2}{\dot{\epsilon}_1} / (\frac{T_2}{T_1} - 1)$$

$C_1 = 7$

$C_2 = 6.61$

$C_3 = 7.47$

$C_4 = 6.75$

$\overline{C} = 6.95 \approx 7$

Table 5. Calculation of the Activation Energy
from the Relationship

$$Q = R \frac{\ell_n \dot{\varepsilon}_2 - \ell_n \dot{\varepsilon}_1}{1/T_2 - 1/T_1}$$

R = 1.9874 cal/mole°K

$T(°K)$	$\dot{\varepsilon}_0 (min^{-1})$	$1/T(°K^{-1})$ $\times 10^{-3}$	$\ell_n \dot{\varepsilon} (min^{-1})$
451	0.27	2.22	-1.3
483	1	2.07	0
506	2	1.97	0.693
523	2.8	1.91	1.03
533	4.2	1.87	1.44
545	5.4	1.834	1.68

$$Q = -1.9874 \left(\frac{cal}{mole°K}\right) \frac{\ell_n 5.4 - \ell_n 1}{1/545 - 1/483} \times 10^3 °K$$

= 14,200 cal/mole.

REFERENCES

1. Sauveur, A., "What is Steel?-Another Answer," Iron Age 113 (February, 1924) 518.

2. Pearson, C. E., "The Viscous Properties of Extruded Eutectic Alloys of Lead-Tin and Bismuth-Tin," Journal Institute of Metals 54, 1 (1934) 111.

3. Bochvar, A. A. and Sviderskaia, Z. A., "Superplasticity Phenomenon in Zinc-Aluminum Alloys," Izv. Akad. Nauk SSSR. Otdel. Tech. Nauk 9 (1945) 821.

4. Presnyakov, A. A. and Chervyakova, V. V.,"On the Subject of "Superplasticity" of Alloys," The Physics of Metals and Metallography (Pergamon Press Translation) 8, 1 (1959) 96.

5. Starikova, G. V. and Presnyakov, A. A., "Metastability of Cast Eutectics Assessed in Connection with the Superplasticity Effect, Physics of Metals and Metallography (Pergamon Press Translations) 13, 5 (1962) 769.

6. Presnyakov, A. A. and Starikova, G. V., "The Relationship Between Rate of Deformation and Solid State Transformation as a Condition for the Occurrence of Superplasticity," Russian Metallurgy and Mining (Scientific Information Consultants Translation) 4 (1963) 95.

7. Chaudhari, P., "Deformation Behavior of Superplastic Zn-Al Alloy," Acta. Metallurgica, 15 (Dec. 1967) 1777.

8. Underwood, E. E., "A Review of Superplasticity," Journal of Metals (December, 1962) 914.

9. Johnson, R. H., "Superplasticity," Metallurgical Reviews, 15 (1970) 115.

10. Davies, G. J., Edington, J. W., Cutler, C. P. and Padmanabhan, K. A., "Superplasticity: A Review," Journal of Materials Science, 5 (1970) 1091.

11. Nicholson, R. B., "The Role of Metallographic Techniques in the Understanding and Use of Superplasticity," in *Electron Microscopy and Structure of Materials*, edited by G. Thomas, R. M. Fulrath, and R. M. Fisher, University of California Press, Berkeley (1972) 689.

12. Backofen, W. A., Turner, I. R. and Avery, D. H. "Superplasticity in an Al-Zn Alloy," *ASM Trans. Quarterly* 57, (1964) 980.

13. Holt, D. L., "The Relation Between Superplasticity and Grain Boundary Shear in the Aluminum-Zinc Eutectoid Alloy," *Transactions of the Metallurgical Society of AIME* 242 (January, 1968) 25.

14. Alden, T. H., "The Origin of Superplasticity in the Sn-5% Bi Alloy," *Acta Metallurgica* 15, (March, 1967) 469.

15. Avery, D. H. and Backofen, W. A., "A Structural Basis for Superplasticity," *ASM Trans. Quarterly* 58, (1965) 551.

16. Holt, D. L. and Backofen, W. A., "Superplasticity in the Al-Cu Eutectic Alloy," *ASM Trans. Quarterly* 59, (1966) 755.

17. Hayden, H. W., Floreen, S. and Goodel, P. D., "The Deformation Mechanisms of Superplasticity," *Metallurgical Trans.* 3 (April, 1972) 833.

18. Raj, R. and Ashby, M. F., "On Grain Boundary Sliding and Diffusional Creep," *Metallurgical Trans.* 2 (April, 1971) 1113.

19. Ashby, M. F. and Verrall, R. A., "Diffusion-Accommodated Flow and Superplasticity," *Acta Metallurgica* 21 (February, 1973) 149.

20. Appendix from Reference 19, "Derivation of Approximate Constitutive Equations for Diffusion Controlled and for Interface-Reaction Controlled Flow."

21. Headly, T. J., Kalish, D. and Underwood, E. E., "The Current Status of Applied Superplasticity," in *Ultra-fine-Grain Metals*, edited by J. J. Burke and V. Weiss, Syracuse University Press, Syracuse, New York (1970) 325.

22. Davies, G. J., Edington, J. W., Cutler, C. P. and Padmanobhan, K. A., "Superplasticity: A Review," *Journal Materials Science* 5 (1970) 1091.

23. Hayden, H. W., Gibson, R. C., Merrick, H. F. and Brophy, J. H., "Superplasticity in the Ni-Fe-Cr System," Trans. ASM, 60 (1967) 3.

24. Hayden, H. W. and Brophy, J. H., "The Interrelation of Grain Size and Superplastic Deformation in Ni-Cr-Fe Alloys," Trans. ASM 61 (1968) 542.

25. Underwood, E. E., Fike, K. D., Kranzlein, H. H., Lee, E. U., and Rack, H. J., "Mechanism of Superplasticity in Al-78% Zn Alloys," Interim Report, Lockheed Georgia Company, (June 30, 1968).

26. Metals Handbook, Volume 8, "Metallographic Methods," American Society for Metals (1973) 1.

27. Kehl, G. L., "The Principles of Metallographic Laboratory Practice," New York and London, McGraw-Hill (1939).

28. DUCTILITY, "Papers presented at a seminar of the American Society for Metal," American Society for Metals, Metals Park, Ohio (October 14 and 15, 1967) 5.

29. Underwood, E. E., Quantitative Stereology, Addison-Wesley, (1970) 81.

30. Appendix from Reference 21, "Metallographic Measurement of Grain Sizes and Grain Boundary Surface Area per Unit Volume."

31. Conrad, H., "Thermally Activated Deformation of Metals," Journal of Metals, (July, 1964) 582.

32. Underwood, E. E., "Interrelationships among High-Temperature Strength and Ductility Criteria," Joint International Conference on Creep, 1963, Paper No. 56.

VITA

I was born on April 15, 1944, in the valley of Logar, Afghanistan. My Bachelor of Science in Mechanical Engineering was earned at the School of Engineering at Kabul University in 1966. I was then employed as a staff member by Kabul University, serving for two years on the Faculty of Medicine, Department of Bio-physics and for an additional two years in the School of Engineering. At both these schools I taught courses as well as coordinated the machine shop. These experiences helped me decide to go to graduate school to broaden my education. In 1971, I was given a scholarship under the United States Engineering Team Program, which enabled me to come to the United States for the purpose of getting a Masters Degree in Mechanical Engineering at the Georgia Institute of Technology.

My future plans are to get a Ph.D. in Mechanical Engineering, to pursue teaching, and to do scientific research.